NUMERICAL MODELING OF DAMAGE PROCESS IN COHESIVE-FRICTIONAL MATERIALS

By Hojjat Mohammadi, B.Sc., M.Sc.

A Thesis Submitted to the School of Graduate Studies in Partial Fulfilment of the Requirement for the Degree Doctor of Philosophy in Civil Engineering

McMaster University DOCTOR OF PHILOSOPHY (2020) Hamilton, Ontario
(Civil Engineering)

TITLE: Numerical Modeling of Damage Process in Cohesive-Frictional Materials

AUTHOR: Hojjat Mohammadi, B.Sc. (Shahid Bahonar University of Kerman), M.Sc. (Sharif University of Technology)

SUPERVISOR: Professor S. Pietruszczak

NUMBER OF PAGES: v, 54.

Abstract

This research is related to modeling of the damage process in cohesive-frictional materials. There are two primary areas of application that include modeling of fractured rock mass as well as some selected topics in biomechanics. For both these areas, the methodology involves a homogenization approach that incorporates volume averaging. The research in rock mechanics deals with the assessment of equivalent mechanical properties of the host rock intercepted by sets of fractures. The effect of fracture network orientation/spacing on the macroscopic strength characteristics is examined. The research in biomechanics has both a numerical and experimental component and is focused on analysis of hip fracture due to a sideways fall. Here, the cortical bone tissue is modeled as a transversely isotropic material and an experimental program is setup to define the anisotropic fracture criterion. In particular, a series of novel direct shear tests is performed on small prism-shaped samples and is accompanied by uniaxial tension and compression performed at different orientations relative to the loading direction. It is demonstrated that the conditions at failure in compression range are independent of confining pressure, while the strength itself is orientation dependent. The failure criteria are postulated using the critical plane approach and the microstructure tensor approach in tension and compression regimes, respectively, and a procedure for identification of material constants is proposed. The last part of this research deals with numerical simulation of fracture propagation in a femur bone subjected to loading conditions simulating a sideways fall. A specific experimental test is modelled, and the mechanical properties of cortical tissue are specified from a series of independent material tests conducted on samples extracted from the fractured femur. The analysis incorporates the newly developed failure criteria and the numerical results pertaining to the assessment of ultimate load and the evolution of fracture pattern are compared with the experimental data.

Acknowledgements

Firstly, I would like to express my sincere gratitude to my advisor Prof. Pietruszczak for the continuous support of my Ph.D. study, for his patience, motivation, and immense knowledge. His priceless guidance helped me a lot at every stage of the research and writing of this thesis. I could not have imagined having a better advisor and mentor in my life.

Besides my advisor, I would like to thank the members of my supervisory committee: Prof. Guo, Prof. Wu, and Dr. Quenneville, not only for their insightful comments and encouragement but also for suggestions to broaden my research in various perspectives.

My sincere thanks also go to my friend Sina, for his help over the course of my graduate studies. In addition, I want to thank my officemates (Amir Arsalan, Roham, Reza) for numerous technical discussions that we had, as well as my friend Kianoosh for his kind offer to read and comment on my thesis. Special thanks also go to the geotechnical lab technician, Peter, who helped me during my experimental tests.

Finally, I would like to thank my wife Faezeh for her love and constant support, for all the late nights and early mornings. She made me much happier during the hard times of the Ph.D. process. I would like to express my gratitude also to my parents, Ahmad & Zahra, without them I could not even start my Ph.D. journey. I owe my parents and my wife everything.

Co-Authorship:

Based on the regulation of "Sandwich" thesis, details of cooperation between authors for each paper are presented here.

Chapter 2:

H. Mohammadi has implemented the embedded discontinuity approach to model a fractured rock mass with some pre-existing cracks and to check for the onset of new crack formation. At all stages of work, the key aspects of the formulation were discussed with Dr. S. Pietruszczak. The framework was then incorporated by him in an FEM code and a series of numerical examples, taken from literature, were solved. This chapter was drafted by H. Mohammadi and revised and finalized by Dr. S. Pietruszczak.

Chapter 3:

Experimental tests, including direct shear, uniaxial tension and uniaxial compression, have been performed by H. Mohammadi on samples of cortical tissue extracted from a bovine femur bone. The objective was to verify the performance of anisotropic fracture criteria based on critical plane and microstructure tensor approach. At all stages of the work, the main aspects of the testing program and its interpretation were discussed with Dr. S. Pietruszczak. A draft of this chapter was prepared by H. Mohammadi, revised and finalized by Dr. S. Pietruszczak.

Chapter 4:

Numerical analysis of an experimental test involving hip fracture due to a sideways fall was carried out. The model of the human femur bone was created from a series of CT scan files, using a commercial software. In addition, some experimental tests were performed to obtain the material constants which were required for the anisotropic models. The UMAT code which has been used for simulations discussed in chapter 2, was enhanced in order to handle complex 3D crack propagation through the femur bone. The numerical results were verified against the experimental data. A draft of this chapter was prepared by H. Mohammadi, revised and finalized by Dr. S. Pietruszczak and Dr. C. Quenneville.

Table of contents

1 Introduction

In this chapter, a summary of research and a brief review of the employed methodologies are presented. The main focus in this work is on numerical modeling of crack growth in fractured rock mass as well as in human femur bone under the event of a sideways fall. In addition, some experimental tests have been performed on both bovine and human femur bone. This thesis is presented in article-based format which includes three journal papers in separate chapters as the main contributions in this study. The list of publications is as follows:

1. Mohammadi, H, and S. Pietruszczak. 2019. "Description of Damage Process in Fractured Rocks." *International Journal of Rock Mechanics and Mining Sciences* 113: 295–302.

2. Mohammadi, H., and S. Pietruszczak. 2020. "Experimental and Analytical Study of Anisotropic Strength Properties of Bovine Cortical Bone." *Biomechanics and Modeling in Mechanobiology*. https://doi.org/10.1007/s10237-020-01319-2.

3. Mohammadi, H., S. Pietruszczak, C. Quenneville. 2020. "Numerical analysis of hip fracture due to a sideways fall." *Journal of Biomechanical Engineering*, submitted.

1.1 Motivation and background

This thesis deals with modeling of the localized damage in cohesive-frictional materials. The class of materials that may be termed as cohesive-frictional is quite broad and includes geomaterials (soils, rocks), some structural materials (e.g., concrete, masonry), as well as certain biomaterials (e.g., bone tissue). This research comprises some aspects of Geomechanics and Biomechanics. The former is focused on examining the behaviour of rock-like materials that contain pre-existing fractures. The topic is of particular relevance to analysis of underground structures (tunnels, shafts, etc.), where the design requires the specification of the Excavation Damage Zone (EDZ). The latter is of utmost importance in the long-term safety assessment of critical engineering structures, such as Deep Geological Repositories of nuclear waste. The research contains several novel elements, including the approach to deal with intersecting cracks and/or formation of new macrocracks in a domain with pre-existing fractures.

The research on Biomechanics deals with the modeling of cortical bone tissue. This is important for examining the fracture process in different types of bones, as well as the issues related to bone-implant interaction. In this work, a novel experimental procedure is employed to formulate and to verify a general form of the fracture criterion. The latter is later applied to study, in a quantitative manner, the onset and propagation of localized damage in a human femur subjected to loading conditions simulating a sideways fall.

The research presented here contains experimental as well as numerical parts. In what follows, a concise literature review is provided first on both these parts in relation to the two main areas of applications mentioned above, i.e. fractured rock mass and biomechanics. Later, the key details on the general scope of work and the contribution are provided.

Fractured Rock Mass

Fractured rock mass is a heterogeneous and anisotropic medium at the macroscale. The existence of fractures affects the mechanical response in two ways. First, there is a reduction of rock mass strength which is triggered by sliding/separation along the cracks. Second, the pre-existing cracks act as stress concentrators triggering the formation of new macrocracks that can propagate through the domain (cf. [1], [2], [3]). Over the last few decades, extensive research has been carried out into the behaviour of fractured rock mass under various loading conditions. The experimental work focused primarily on examining the effect of pre-existing flaws on the response under uniaxial as well as biaxial compression.

In parallel with experimental work, a significant amount of research has been conducted on numerical analysis of crack growth and propagation. Since the advent of the computational era in the 1960's, various approaches have emerged for modelling the initiation and propagation of cracks in engineering materials. The technique used in early references ([4], [3]) incorporated separation of the edges of elements. Another approach was the smeared crack model as proposed by Rashid in the late 1960's [5]. The latter was widely used in modelling of damage because of its simplicity within FEM formulation. At the same time, however, the results did not prove to be reliable because of a strong dependency of the solution on the FE discretization.

An alternative methodology for dealing with discrete propagation of crack involves the boundary element method (BEM). Unlike the FEM, which results in a symmetric, banded system of equations [6], the BEM approach generally leads to a non-symmetric, congestive equation system. The first FEM approach, which enforces the mesh objectivity was that developed in reference [7]. It was based on a smeared representation incorporating volume averaging. The formulation was later enhanced by introducing a "characteristic dimension" which was explicitly related to geometry of the discretized domain [8].

Biomechanics

Both cortical and trabecular bone tissues have a complex heterogeneous microstructure that results in an inherent anisotropy of mechanical properties at a macroscale (cf. [9]). Over the last few decades, extensive experimental work was undertaken to investigate those properties. For trabecular bone, it is difficult to obtain consistent quantitative results as the mechanical response changes with the anatomical location ([10], [11]). Therefore, the literature on the specification of the mechanical properties is more exhaustive for the cortical bone. The latter plays a primary role in bearing physiological and other forms of loads. The most comprehensive and representative experimental study on cortical bone is perhaps that reported in ref. [12]. The published data typically involves the results of uniaxial tension as well as compression and is focused on the assessment of both the strength and stiffness; the latter also in the inelastic range (cf. [13]). An extensive overview of the existing experimental techniques is provided in ref. [14]. It is interesting to note that shear behavior is usually tested by an indirect approach using structural elements. In ref. [15], notched beam specimens were tested under the vertical load that created zero bending moment across the notch. In ref. [16], the shear was caused by placing tensile axial load on elongated specimens with asymmetric double-notch. Ref. [17] also used a double-notched specimen; however, in the latter case the shear configuration involved testing inclined samples under compressive axial load. The interpretation of these tests may be open to question, as they actually represent the boundary value problems. A similar conclusion applies to torsional tests on prismatic bars (cf.[18]). The pure shear tests reported in ref. [19] appear to be the only type of material tests conducted so far to examine the shear characteristics.

In terms of constitutive modelling of cortical bone, one of the first attempts was a lower and upper bound evaluation of elastic moduli based on mechanics of composite materials [20]. Later, many micromechanical approaches were adopted for determining elastic properties and ultimate axial stress ([21],[22]). Though robust, these concepts were not tested and/or implemented in the sense of the structural analysis of whole bones. A significant research effort has also been directed towards the description of the onset of fracture in trabecular bone and the specification of conditions at failure ([23], [24], [25]). More recently, an extensive experimental and analytical studies on multiaxial response of trabecular bone were performed (cf. [26]). Generally, the primary challenge in describing the conditions at failure in trabecular tissue is the fact that trabeculae architecture strongly depends on anatomical position so that the definition of anisotropy requires specific fabric descriptors. This is different from cortical bone where the principal material axes can be identified *a priori* based on the cortical shell geometry.

In terms of numerical modeling, a number of researchers focused on simulation of hip fracture, which is one of the most common injury in elderly population, inducing morbidity and loss of life [27]. The analysis incorporated subject-specific FEM models based on quantitative Computed Tomography ([28], [29], [30], [31], [32]). Most of these models were verified against *ex-vivo* mechanical tests and some were found to produce better estimates of femoral strength and/or fracture load than the BMD evaluation ([30], [33]). In most cases there were no separate laboratory tests to evaluate the actual mechanical properties.

More recent studies on femoral fracture involve attempts to describe the crack initiation and propagation. Cohesive zone elements ([34], [35]), homogenized voxel models at continuum level [28], continuum damage mechanics methods including the elimination of cracked elements ([36], [37]), as well as Extended Finite Element Method (XFEM) have been employed. Except XFEM, the other mathematical frameworks provide results which are mesh-dependent. XFEM approach has attracted a lot of attention in numerical simulation of tensile fracture of biomaterials. For instance, in refs. ([25], [38]) the authors employed XFEM to trace crack and its propagation in a human femoral bone. The incorporation of discontinuities in XFEM requires additional degrees of freedom around a cracked region. Moreover, the integration schemes are often vulnerable to divergence when dealing with fracture patterns involving the propagation of long single cracks and/or several intersecting cracks ([38], [39]).

1.2 General scope of work and contribution

In this section an overview of the material covered in each chapter is provided, together with some comments on the contribution in each study. As mentioned earlier, the individual chapters of this thesis are associated with journal articles that address the main research topics.

In Chapter 2, description of damage process in fractured rocks is discussed. This chapter is focused on the study of the damage propagation in rock mass that contains several pre-existing fractures. The methodology employs an enhanced embedded discontinuity approach which is extended here to take into account the existence of multiple sets of joints. The framework can be easily implemented in standard FE platform and the results are independent of the mesh size / alignment. The method is shown to be able to predict complex fracture modes associated with the initiation and propagation of new cracks within the region containing the pre-existing fractures.

The main novelty of research reported in Chapter 2 is the use of volume averaging approach to deal with damage propagation in case of multiple intersecting cracks. In this case, the use of XFEM platform would be computationally very costly and there are no applications dealing with this class of problems.

In Chapter 3, the results of an experimental and analytical study of anisotropic strength properties of bovine cortical bone are provided. This chapter is focused on determining conditions at failure in cortical tissue under a general state of stress. The experimental part involves a series of innovative direct shear experiments that examine the sensitivity of the shear strength to normal stress for samples tested at different orientation. The study is accompanied by standard axial compression and tension tests to establish a general form of the failure criterion. The analytical part describes two different approaches for evaluating the anisotropic strength criterion, i.e. critical plane approach and microstructure tensor approach. A procedure for determining material parameters is discussed which incorporates the results of the material tests conducted.

The major novel aspects of the study in Chapter 3 is the use of a direct shear test to determine the conditions at failure in a cortical bone. To the authors' knowledge, this is the first experimental evidence that the failure in compression regime for cortical bone is independent of the confining pressure (i.e. hydrostatic stress). It has also been demonstrated that the strength anisotropy requires an adequate mathematical representation as it does not follow standard transformation rules.

In Chapter 4, the numerical analysis of hip fracture due to a sideways fall is presented. The primary purpose of this chapter is to describe a method for evaluating the probability of cortical bone fracture in the proximal femur in the event of a sideways fall. The method consists of conducting FE analyses in which the cortical bone is treated as an anisotropic material and verifying the plastic admissibility of the stress field. Two methodologies are used in assessing the initiation of fracture, i.e. Critical Plane approach and the Microstructure Tensor approach. The former is used in the tension, while the latter in compression regime. A constitutive law with embedded discontinuity (CLED) is used to model the propagation of localized damage. In order to define the material properties, a series of independent experimental tests has been performed on cortical bone samples tested at different orientation. The numerical analysis deals with simulation of the sideways fall and the results are compared with the experimental data. This includes evolution of crack pattern and load-displacement characteristics.

The research in Chapter 4 has elements of novelty that include the implementation of the new fracture criteria to assess, in a quantitative way, the fracture load in a femur bone due to a sideways fall. The approach is fairly comprehensive as it includes the specification of bone geometry based on clinical CT scan data, conducting a series of tests to determine the appropriate material properties and the numerical simulations of a fracture test incorporating an advanced technique for tracing the crack propagation.

It should be mentioned that for conducting the research, the mathematical formulation presented here has been implemented in user material subroutine (UMAT) of the commercial software Abaqus. This includes the governing constitutive relations as well as the crack propagation algorithm. Finally, it needs to be mentioned that given the format of this thesis, which includes three separate journal papers, there is a certain overlap in terms of describing the details of the formulation. This cannot be avoided in a sandwich type of presentation.

1.3 References

[1] A. Bobet, "Fracture coalescence in rock materials: experimental observations and numerical predictions," 1997.

[2] A. V. Dyskin, E. Sahouryeh, R. J. Jewell, H. Joer, and K. B. Ustinov, "Influence of shape and locations of initial 3-D cracks on their growth in uniaxial compression," Eng. Fract. Mech., vol. 70, no. 15, pp. 2115–2136, 2003.

[3] Y.-P. Li, L.-Z. Chen, and Y.-H. Wang, "Experimental research on pre-cracked marble under compression," Int. J. Solids Struct., vol. 42, no. 9–10, pp. 2505–2516, 2005.

[4] C. H. Park and A. Bobet, "Crack initiation, propagation and coalescence from frictional flaws in uniaxial compression," Eng. Fract. Mech., vol. 77, no. 14, pp. 2727–2748, 2010.

[5] P. Cao, T. Liu, C. Pu, and H. Lin, "Crack propagation and coalescence of brittle rock-like specimens with pre-existing cracks in compression," *Eng. Geol.*, vol. 187, pp. 113–121, 2015.

[6] M. Sagong and A. Bobet, "Coalescence of multiple flaws in a rock-model material in uniaxial compression," *Int. J. Rock Mech. Min. Sci.*, vol. 39, no. 2, pp. 229–241, 2002.

[7] S. Pietruszczak and Z. Mroz, "Finite element analysis of deformation of strain-softening materials," *Int. J. Numer. Methods Eng.*, vol. 17, no. 3, pp. 327–334, 1981.

[8] S. Pietruszczak, "On homogeneous and localized deformation in water-infiltrated soils," *Int. J. Damage Mech.*, vol. 8, no. 3, pp. 233–253, 1999.

[9] R. B. Martin, D. B. Burr, N. A. Sharkey, and D. P. Fyhrie, *Skeletal Tissue Mechanics*, Second Edi. New York, 2016.

[10] A. Odgaard and F. Linde, "The underestimation of Young's modulus in compressive testing of cancellous bone specimens," *J. Biomech.*, vol. 24, no. 8, pp. 691–698, 1991.

[11] T. M. Keaveny, T. P. Pinilla, P. R. Crawford, D. L. Kopperdahl, and A. Lou, "Systematic and Random Errors in Compression Testing of Trabecular Bone," *J. Orthop. Res.*, vol. 15, no. 1, pp. 101–110, 1997.

[12] D. T. Reilly and A. H. Burstein, “The elastic and ultimate properties of compact bone tissue,” *J. Biomech.*, vol. 8, no. 6, pp. 393–405, 1975.

[13] J. S. Nyman, H. Leng, X. N. Dong, and X. Wang, “Differences in the mechanical behavior of cortical bone between compression and tension when subjected to progressive loading,” *J. Mech. Behav. Biomed. Mater.*, vol. 2, no. 6, pp. 613–619, 2009.

[14] R. Zdero, *Experimental Methods in Orthopaedic Biomechanics*. Academic Press, 2017.

[15] K. Winwood, P. Zioupos, J. D. Currey, J. R. Cotton, and M. Taylor, “Strain patterns during tensile , compressive , and shear fatigue of human cortical bone and implications for bone biomechanics,” *J. Biomed. Mater. Res.*, vol. 79, no. 2, pp. 289–297, 2006.

[16] S. Saha, “Longitudinal shear properties of human compact bone and its constituents , and the associated failure mechanisms,” *J. Mater. Sci.*, vol. 12, pp. 1798–1806, 1977.

[17] X. N. Dong, Q. Luo, and X. Wang, “Progressive post-yield behavior of human cortical bone in shear,” *Bone*, vol. 53, no. 1, pp. 1–5, 2013.

[18] H. C. Park and R. S. Lakes, “Cosserat micromechanics of human bone: strain redistribution by a ydration sensitive constituent,” *J. Biomech. Eng.*, vol. 19, no. 5, pp. 385–397, 1986.

[19] C. H. Turner, T. Wang, and D. B. Burr, “Shear Strength and Fatigue Properties of Human Cortical Bone Determined from Pure Shear Tests,” *Clacified Tissue Int.*, vol. 69, pp. 373–378, 2001.

[20] K. Piekarski, “Analysis of bone as a composite material,” *Int. J. Eng. Sci.*, vol. 11, no. 6, pp. 557–565, 1973.

[21] I. Jäger and P. Fratzl, “Mineralized collagen fibrils: A mechanical model with a staggered arrangement of mineral particles,” *Biophys. J.*, vol. 79, no. 4, pp. 1737–1746, 2000.

[22] H. Gao, B. Ji, I. L. Jager, E. Arzt, and P. Fratzl, “Materials become insensitive to flaws at nanoscale: Lessons from nature,” *Proc. Natl. Acad. Sci. U. S. A.*, vol. 100, no. 10, pp. 5597–5600, 2003.

[23] S. W. Tsai and E. M. Wu, “A general theory of strength for anisotropic materials,” *J. Compos. Mater.*, vol. 5, no. 1, pp. 58–80, 1971.

[24] S. C. Cowin, “Fabric dependence of an anisotropic strength criterion,” *Mech. Mater.*, vol. 5, pp. 251–260, 1986.

[25] M. Marco, E. Giner, R. Larraínzar-garijo, J. R. Caeiro, and M. H. Miguélez, “Numerical modelling of femur fracture and experimental validation using bone simulant,” *Ann. Biomed. Eng.*, vol. 45, no. 10, pp. 2395–2408, 2017.

[26] L. Rincón-Kohli and P. K. Zysset, “Multi-axial mechanical properties of human trabecular bone,” *Biomech. Model. Mechanobiol.*, vol. 8, no. 3, pp. 195–208, 2009.

[27] O. Johnell and J. A. Kanis, "An estimate of the worldwide prevalence and disability associated with osteoporotic fractures," *Osteoporos. Int.*, vol. 17, no. 12, pp. 1726–1733, 2006.

[28] E. D. Ara, B. Luisier, R. Schmidt, F. Kainberger, P. Zysset, and D. Pahr, "A nonlinear QCT-based finite element model validation study for the human femur tested in two configurations in vitro," *Bone*, vol. 52, pp. 27–38, 2013.

[29] J. H. Keyak, S. A. Rossi, K. A. Jones, C. M. Les, and H. B. Skinner, "Prediction of fracture location in the proximal femur using finite element models," *Med. Eng. Phys.*, vol. 23, no. 9, pp. 657–664, 2001.

[30] D. Dragomir-Daescu *et al.*, "Robust QCT/FEA models of proximal femur stiffness and fracture load during a sideways fall on the hip," *Ann. Biomed. Eng.*, vol. 39, no. 2, pp. 742–755, 2011.

[31] L. Grassi *et al.*, "Accuracy of finite element predictions in sideways load configurations for the proximal human femur," *J. Biomech.*, vol. 45, no. 2, pp. 394–399, 2012.

[32] J. E. M. Koivumäki *et al.*, "Ct-based finite element models can be used to estimate experimentally measured failure loads in the proximal femur," *Bone*, vol. 50, no. 4, pp. 824–829, 2012.

[33] D. D. Cody, G. J. Gross, F. J. Hou, H. J. Spencer, S. A. Goldstein, and D. P. Fyhrie, "Femoral strength is better predicted by finite element models than QCT and DXA," *J. Biomech.*, vol. 32, pp. 1013–1020, 1999.

[34] A. Ural, P. Bruno, B. Zhou, X. T. Shi, and X. E. Guo, "A new fracture assessment approach coupling HR-pQCT imaging and fracture mechanics-based finite element modeling," *J. Biomech.*, vol. 46, no. 7, pp. 1305–1311, 2013.

[35] A. Ural and S. Mischinski, "Multiscale modeling of bone fracture using cohesive finite elements," *Eng. Fract. Mech.*, vol. 103, pp. 141–152, 2013.

[36] R. Hambli, A. Bettamer, and S. Allaoui, "Finite element prediction of proximal femur fracture pattern based on orthotropic behaviour law coupled to quasi-brittle damage," *Med. Eng. Phys.*, vol. 34, no. 2, pp. 202–210, 2012.

[37] R. Hambli, "A quasi-brittle continuum damage finite element model of the human proximal femur based on element deletion," *Med. Biol. Eng. Comput.*, vol. 51, pp. 219–231, 2013.

[38] M. Marco, E. Giner, J. R. Caeiro-rey, M. H. Miguélez, and R. Larraínzar-garijo, "Numerical modelling of hip fracture patterns in human femur," *Comput. Methods Programs Biomed.*, vol. 173, pp. 67–75, 2019.

[39] A. A. Ali *et al.*, "Specimen-specific modeling of hip fracture pattern and repair," *J. Biomech.*, vol. 47, no. 2, pp. 536–543, 2014.

International Journal of Rock Mechanics and Mining Sciences 113 (2019) 295–302

Contents lists available at ScienceDirect

International Journal of Rock Mechanics and Mining Sciences

journal homepage: www.elsevier.com/locate/ijrmms

Description of damage process in fractured rocks

H. Mohammadi, S. Pietruszczak*

McMaster University, Hamilton, Ontario, Canada

ARTICLE INFO

Keywords:
Fractured rock mass
Embedded discontinuities
Volume averaging

ABSTRACT

This paper is focused on analysis of the damage process in rock that contains some pre-existing fractures. The methodology employs an enhanced embedded discontinuity approach, which is extended here to account for the presence of multiple sets of joints. The approach can be easily implemented in standard FE codes and the results are virtually independent of mesh size/alignment. This is in view of incorporation of a 'characteristic dimension' which explicitly depends on discretization of the domain. It is demonstrated that the approach is capable of predicting complex fracture modes associated with formation and propagation of new cracks within the region that contains the pre-existing flaws.

1. Introduction

A fractured rock mass is a heterogeneous and, in general, an anisotropic medium at the macroscale. The existence of fractures has two predominant effects on the mechanical response. The first one is the reduction of strength of rock mass that is triggered by sliding/separation along the defects. Secondly, the pre-existing cracks act as stress concentrators prompting the formation of new macrocracks that may propagate through the domain (cf. ref.1–3). Over the last few decades, extensive research has been conducted on the behaviour of fractured rock mass under variable loading conditions. The experimental work focused mainly on investigating the effect of pre-existing flaws on the response under uniaxial as well as biaxial compression. In ref.4, a series of uniaxial compression tests has been performed to study the crack propagation and coalescence. The authors used gypsum specimens with pre-existing cracks (flaws) and examined the response for different geometries of flaws. The main conclusion of their research was that the fracturing process for closed and open flaws was very similar. The research reported in ref.5 and ref.6, also dealt with axial compression in the presence of pre-existing cracks. In the former reference the samples were prepared using a mixture of fine sand and cement mortar, while in the latter the gypsum specimens were tested. In both cases, the authors examined the influence of the flaw inclination angle as well as the spacing between cracks on the predominant failure mode that involved the crack coalescence. The study conducted in ref.7 comprised the uniaxial as well as biaxial compression tests on pre-fractured rock-like material that contained both the open as well as closed flaws. The authors noted that as the vertical load was increasing new cracks would form at the tip of the existing flaws and propagate until eventual coalescence. The location of the onset of a wing crack would strongly depend on the confining pressure. Further experimental studies on the growth and coalescence of fractures under compressive/shear loads have been reported in ref.8 and ref.9. The results showed that the inclined parallel flaws can coalesce in shear and/or tensile mode, which is highly depend on relative position of cracks in relation to the direction of loading. A similar study was conducted in ref.10, whereby the evolution of crack pattern in axial compression tests was tracked, both at macro and microscales, in specimens of gypsum and marble containing pre-existing open flaws of different geometric configurations.

In parallel with experimental work, a significant amount of research has been conducted on numerical analysis of crack growth and propagation. The existing literature in this respect is too extensive to provide a comprehensive review. Therefore, only a brief and limited overview of different methodologies is given here. The very first approach was based on separation of element edges.[11,12] The subsequent approach, initiated by Rashid in the late 1960's,[13] incorporated the notion of a 'smeared crack'. Both these methodologies resulted in a mesh size dependency, which was a significant constraint. In order to address the problem, a conceptually different approach has been introduced by Pietruszczak and Mroz,[14] and was later reformulated.[15] This methodology was based on enhancement in the constitutive relation, which incorporated an embedded discontinuity and the associated 'characteristic dimension'. The approach has been shown to be independent of discretization and will be employed in the research reported here. The most notable subsequent development was the introduction of Extended Finite Element Method (XFEM), in which additional degrees of freedom were incorporated to reflect the presence of discontinuities associated with the onset and propagation of fracture within the finite element framework.

In relation to rock mechanics, examples of description of damage

* Corresponding author.

https://doi.org/10.1016/j.ijrmms.2018.12.003
Received 17 April 2018; Received in revised form 15 November 2018; Accepted 4 December 2018
Available online 20 December 2018
1365-1609/

process in the presence of pre-existing cracks include the research reported in ref.16 and ref.17. In ref.16, the authors employed an energy balance algorithm to envisage the crack propagation in brittle regime. In ref.17, the Discrete Element Method, employing a bonded-particle model for pre-fractured specimens, was used to investigate the crack coalescence under uniaxial compression. The authors concluded that the coalescence and the peak strength of samples strongly depend on the crack inclination angle, spacing between cracks, and bridging angle between flaws. In ref.18, the rock failure process analysis (RFPA) code, incorporating elastic damage mechanics, was employed to examine the propagation/coalescence of cracks in brittle rocks. It was found that under axial compression wing-cracks would initiate from the tip of pre-existing cracks and propagate throughout the domain. The authors also demonstrated that in the presence of confining pressure, crack propagation will be stable and will stop at some finite length.

The research reported in this work deals with frictional crack propagation. It employs a different and simpler methodology that incorporates an enhanced embedded discontinuity approach. The latter originates from ref.19 and is conceptually similar to that outlined in ref.15. In what follows an extension of this framework is first presented for the case of pre-existing sets of fractures within the rock mass. A volume averaging scheme, often employed for upscaling purposes (cf. ref.20), is then invoked to define the macroscopic properties. The approach is applied to simulate a series of compression tests on a pre-fractured rock-like samples. Various geometric configurations of pre-existing cracks are considered and the results are compared with the experimental data. It is demonstrated that the advocated approach, which is simple and physically appealing, is quite adequate to describe the process of discontinuous damage within the rock mass in the presence of pre-existing fractures.

2. Formulation incorporating the volume averaging approach

Fig. 1 shows a schematic picture of rock mass which contains two sets of joints embedded within the intact material. The joints have spacing $s^{(i)}$ and the thickness $h^{(i)}$, where $i = 1, 2$. In this case, the damage process will comprise sliding/separation along the joints as well as the deformation of the intact rock. Note that the latter may also result in the onset and propagation of new macrocracks that may form within the domain. Assume that the intact rock is an isotropic (or transversely isotropic) elastic-brittle material and consider first the scenario when the deformation is localized along the pre-existing joints. In order to specify the constitutive relation, define the macroscopic strain rate in terms of volume averages of those in the constituents, i.e.

$$\dot{\varepsilon} = \dot{\varepsilon}^{(0)} + \upsilon^{(1)}\dot{\varepsilon}^{(1)} + \upsilon^{(2)}\dot{\varepsilon}^{(2)} \tag{1}$$

Here, the superscript (0) refers to the intact material and υ's are the respective volume fractions of the joint sets. All strain operators are referred to the global coordinate system (Fig. 1). The predominant deformation mode in joints is the plastic deformation, so that the strain

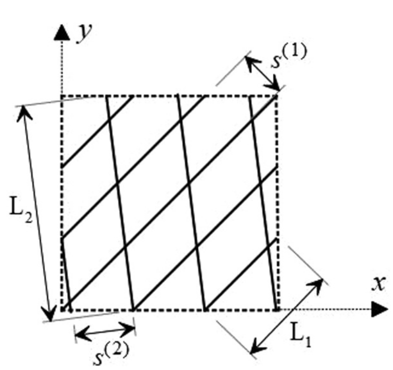

Fig. 1. Geometry of the problem.

rate can be defined in terms of a symmetric part of a dyadic product of unit normal $\boldsymbol{n}$ and the plastic part of velocity discontinuity $\dot{\boldsymbol{g}}^p$. Thus,

$$\dot{\varepsilon}^{(1)} = \frac{1}{h^{(1)}}(\dot{\boldsymbol{g}}^{p(1)} \otimes \boldsymbol{n}^{(1)})^s; \quad \dot{\varepsilon}^{(2)} = \frac{1}{h^{(2)}}(\dot{\boldsymbol{g}}^{p(2)} \otimes \boldsymbol{n}^{(2)})^s \tag{2}$$

where $h^{(1)}$ and $h^{(2)}$ denote the thickness of the two sets of joints.

The equilibrium of traction along the interface and the constitutive relations for all constituents may be written in the general form

$$\begin{aligned}&\dot{\boldsymbol{t}}^{(1)} = \boldsymbol{n}^{(1)}\cdot\dot{\boldsymbol{\sigma}}\,; \quad \dot{\boldsymbol{t}}^{(2)} = \boldsymbol{n}^{(2)}\cdot\dot{\boldsymbol{\sigma}}\\ &\dot{\varepsilon}^{(0)} = \mathbb{C}:\,\dot{\boldsymbol{\sigma}}\,; \quad \dot{\boldsymbol{g}}^{p(1)} = \dot{\boldsymbol{t}}^{(1)}\cdot\boldsymbol{K}^{(1)}; \quad \dot{\boldsymbol{g}}^{p(2)} = \dot{\boldsymbol{t}}^{(2)}\cdot\boldsymbol{K}^{(2)}\end{aligned} \tag{3}$$

where $\mathbb{C}$ is the elastic compliance operator for the intact material, and $\boldsymbol{K}$'s are the joints' compliances. Using the equations above, the following relation between stress and strain rates can be obtained after some algebraic manipulations

$$\begin{aligned}\dot{\varepsilon} = \mathbb{C}:\,\dot{\boldsymbol{\sigma}} &+ \mu^{(1)}((\boldsymbol{K}^{(1)}\cdot\dot{\boldsymbol{\sigma}}\cdot\boldsymbol{n}^{(1)}) \otimes \boldsymbol{n}^{(1)})^s\\ &+ \mu^{(2)}((\boldsymbol{K}^{(2)}\cdot\dot{\boldsymbol{\sigma}}\cdot\boldsymbol{n}^{(2)}) \otimes \boldsymbol{n}^{(2)})^s\end{aligned} \tag{4}$$

In Eq. (4), $\mu^{(1)} = \upsilon^{(1)}/h^{(1)}$ and $\mu^{(2)} = \upsilon^{(2)}/h^{(2)}$, so that

$$\mu^{(1)} = \upsilon^{(1)}/h^{(1)} \simeq \left(\frac{h^{(1)}\ \sum L_1}{s^{(1)}\ \sum L_1}\right)/h^{(1)} \simeq \frac{1}{s^{(1)}}\,; \qquad \mu^{(2)} \simeq \frac{1}{s^{(2)}} \tag{5}$$

where $\sum L$ is the sum of the respective length segments of the joint set. It is noted that when the joints are equally spaced, i.e. $s^{(1)} = s^{(2)} = s$, there is $\mu^{(1)} = \mu^{(2)} = 1/s$. At the same time, for a single set of joints, $\mu^{(1)} = \mu = 1/s\,; \quad \mu^{(2)} = 0$, whereas in case of a single macrocrack embedded in the considered referential volume one has

$$\mu = \frac{V_{cr}}{V\,h} = \frac{A_{cr}}{V} \tag{6}$$

where V_{cr}, A_{cr} is the volume and the cross-sectional area of the macrocrack, respectively, and V is the total referential volume. It is evident that in all cases, the parameter μ is independent of h. The inverse of this parameter, i.e. the dimension μ^{-1}(in units of length) is referred to as the 'characteristic dimension'. It should be pointed out that the averaging domain V, i.e. the referential volume, is identified here with that of the finite element in which localization occurs. Therefore, its size depends on the discretization of the system and the characteristic dimension, viz. Eq. (6), is in fact an explicit function of it. It should also be noted that, for a single fracture, the averaging domain may be considered as 'the neighbourhood of the crack', whereas for multiple joints the notion of referential volume requires the spacing, s, to be small compared to other dimensions.

The implementation of Eq. (4) entails the specification of the compliance operator $\boldsymbol{K}$ for both sets of joints. Referring the problem now to the local coordinate system, such that x_1-axis is normal to the joint, the yield function can be assumed in the form consistent with Coulomb criterion, i.e.

$$f = \tau + \eta\,\sigma_n - c = 0\,; \quad \eta = \tan\phi; \quad \eta = \eta(\kappa) \tag{7}$$

where $\eta = \eta(\kappa)$ is the softening function and $c = const$. The softening parameter κ is identified here with the norm of the tangential component of plastic part of velocity discontinuity and the degradation function $\eta = \eta(\kappa)$ is taken as

$$\eta = \eta_r + (\eta_0 - \eta_r)\,e^{-\beta\,\kappa}; \quad \kappa = \int \sqrt{(\dot{g}_2^p)^2 + (\dot{g}_3^p)^2}\,dt \tag{8}$$

Here, η_0 and η_r correspond to the initial and residual values of the friction angle ϕ, and β is a material constant. Note that the latter controls the gradient of the softening characteristic and it can, in general, be identified by performing a direct shear test along the fracture. Given the expressions above, the operator $\boldsymbol{K}$ can be established following a standard plasticity formalism.

Table 1
Samples and corresponding joint configurations.

Sample	A3	B3	B4	C1	D1
Dip angles (°)	30	30,60	45,45	0,60	0,45,90

3. Numerical examples

The mathematical framework presented in the previous section has been applied to simulate a series of experimental tests discussed in ref.21. The tests involved samples subjected to axial compression in the presence of pre-existing fractures. The rock-like material tested was a mixture of Portland cement (29% by weight), dry river sand (58%) and water (13%). In order to create weakness planes, the steel slices were inserted into a homogeneous mixture and removed 12 h later. The mixture was then cured for 28 days (at room temperature). After that the joints were glued with an epoxy resin adhesive and the cylindrical samples were prepared using a core-drilling machine. Four series A–D of samples with different joint orientation were tested. The numerical simulations conducted here involved a number of tests for which the details on the orientation of joints are provided in Table 1.

For numerical simulations, the samples were discretized using four-noded linear tetrahedral elements. The bottom surface was fixed in the vertical direction, and the out-of-plane nodes along the centre line of this surface were also constrained against the horizontal movement. The loading process consisted of applying the vertical displacements at the top surface. The intact material was assumed to be elastic prior to the onset of macrocracking; the latter defined by the standard Mohr-Coulomb criterion. The response along the new and pre-existing crack was described using the representation (7) and (8), while the procedure for tracing the crack propagation was similar to that used in ref.22. Based on the information provided in the original article,21 the following material parameters were assigned for the intact material:

$$E = 20.2MPa;\ \upsilon = 0.2;\ \varphi = 40^{\circ};\ c = 11MPa \tag{9}$$

for the fractures:

$$k_N = 19.8\ GPa/m;\ k_T = 4.9\ GPa/m;\ \varphi_0 = 36^{\circ}$$
$$\varphi_r = 0.6\varphi_0;\ \ c = 3.22MPa;\ \ \beta = 100m^{-1} \tag{10}$$

Here, $k_N,\ k_T$ are the elastic stiffness coefficients required for verifying the plasticity criterion (7). The strength parameters c and φ for the intact material, which were not provided in the original paper, were estimated based on the value of the uniaxial compressive strength, which was reported to be $47MPa$. Furthermore, the value of φ_r was assumed as $0.6\varphi_0$, which is consistent with experimental results given in ref.23. Note that there was no information provided on the value of the softening parameter β, Eq. (8). Therefore, some parametric studies have been performed to assess its influence on the results of simulations.

3.1. Numerical simulation for sample A3

The first example deals with the axial compression of sample A3, which contains one pre-existing crack with a dip angle of 30^0. The evolution of the fracture pattern is shown in Fig. 2. Here, the pre-existing crack is shown in light pink colour, while the cracks experiencing an active loading process (i.e. plastic deformation) are shown in dark red. Initially, the material remains in the elastic range (cf. figure on the left). As the vertical displacement increases, the elements along the pre-existing crack become gradually activated, i.e. the plasticity criterion (7) is met. At some point, a new fracture forms and propagates towards the pre-existing joint. It is noted that in order to enforce a discrete propagation pattern for this macro-fracture, an imperfection was introduced in one of the elements (i.e. the friction angle was reduced to 35^0). The last figure on the right shows the failure mode associated with the ultimate load.

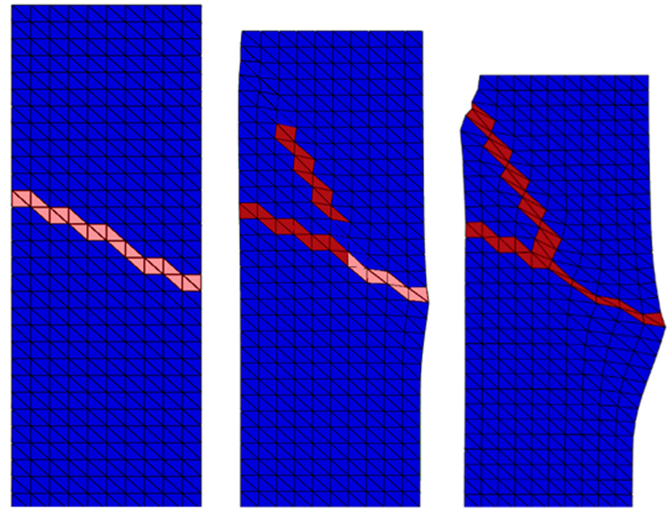

Fig. 2. The predicted evolution of fracture pattern in sample A3 (light pink: the pre-existing crack; dark red: an active crack). (For interpretation of the references to color in this figure legend, the reader is referred to the web version of this article.).

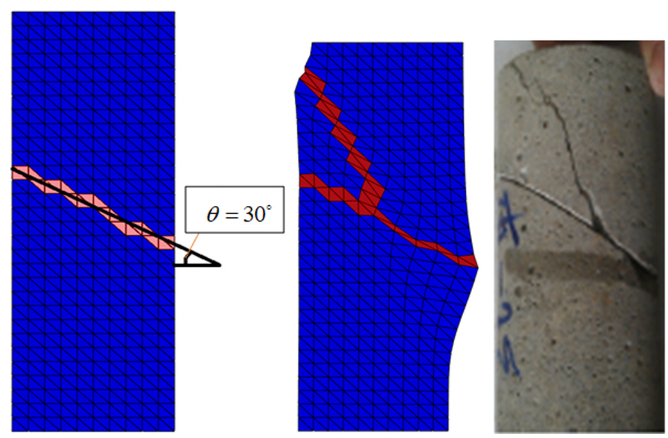

Fig. 3. Comparison of the fracture mode with the experimental results for sample A3.

Fig. 3 shows the comparison of the fracture mode with the actual experimental data. It is evident that the results of simulations are fairly consistent with the observed mechanism. The latter also involves the onset and propagation of a new macrocrack. It is noted that, in the numerical analysis, the direction of new crack in each consecutive element was assumed to be at $45^0 + \varphi/2$ with respect to the direction of minor principal stress, which is implied by the Mohr–Coulomb criterion.

Fig. 4 shows the average stress–strain characteristic for the sample. The behaviour is virtually linear up to the ultimate peak load after which the global response becomes unstable. The predicted ultimate load is fairly consistent with the experimental data.

The last figure here, i.e. Fig. 5, shows the influence of the value of strain-softening parameter β on the stress–strain response. As mentioned earlier, the assumed value of β is rather speculative as no experimental data is available in this respect. It is evident that the value of this parameter affects the slope of the post-critical response; however, it has very little influence on the prediction of ultimate load. It should be pointed out that the simulations shown in Figs. 4 and 5 were terminated after reaching the post-critical range. Since in the present formulation the crack is traced in a discrete manner, there was no loss of convergence. The latter is typically associated with a 'smeared approach' which requires the use of special iterative schemes in the post-critical

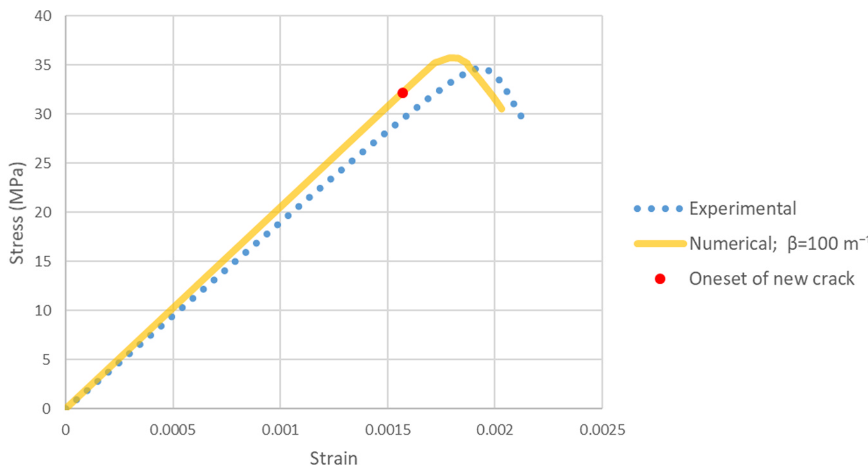

Fig. 4. Average stress–strain curve for sample A3.

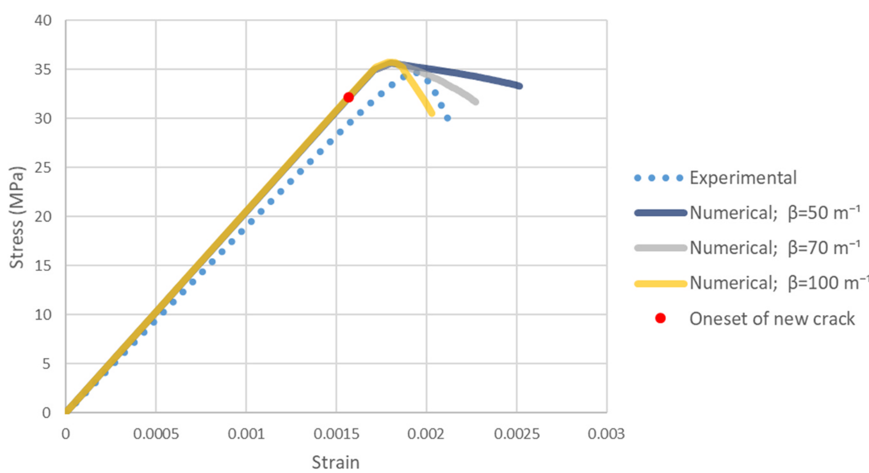

Fig. 5. Influence of the value of parameter β on the mechanical characteristic (sample A3).

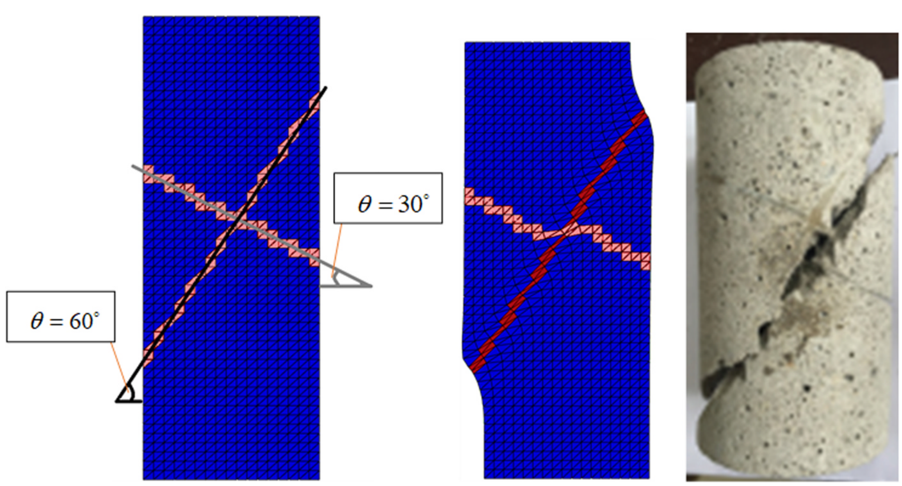

Fig. 6. Comparison of the fracture mode with the experimental results for sample B3.

regime (e.g., an arc-length procedure).

3.2. Numerical simulation for sample B3

The second example deals with the specimen B3 that is subjected to axial compression. This sample contains two pre-existing cracks; one with 30° and the other one with 60° dip angles with respect to horizontal. In this case, the latter crack, i.e that at 60° dip, is activated first and as the load increases, a progressive sliding takes place along this joint. The associated failure mode is consistent with the experimental data, which is evidenced in Fig. 6. The average stress-strain characteristic, as shown in Fig. 7, displays again an unstable (strain softening) response and the predicted ultimate load, as well as the post critical modulus, are very close to those recorded in the test.

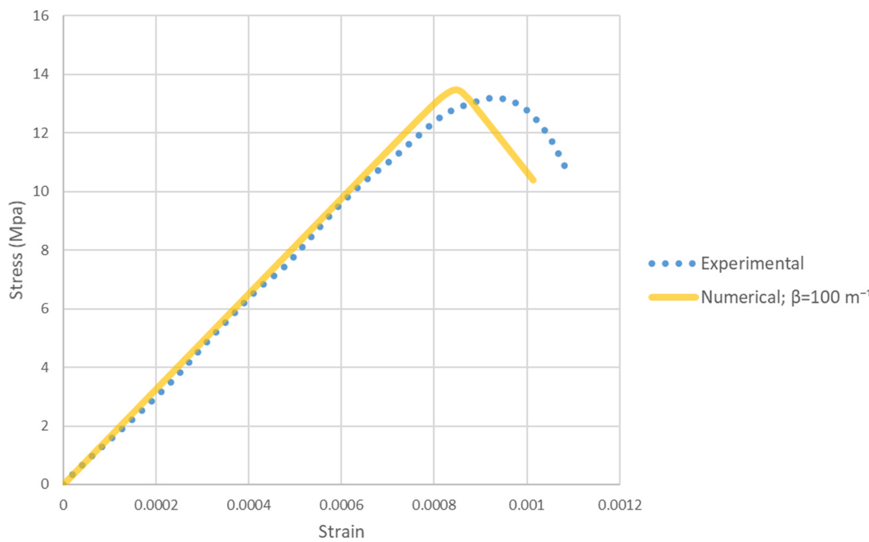

Fig. 7. Average stress–strain curve for sample B3.

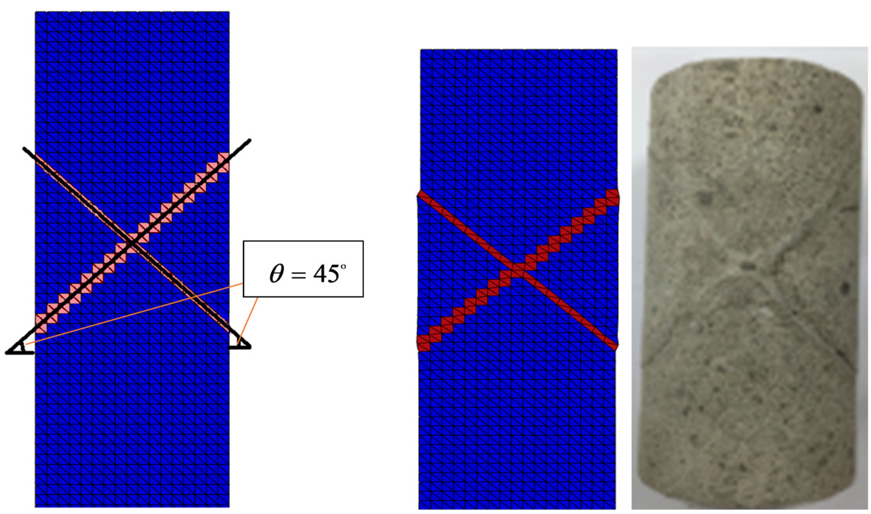

Fig. 8. Comparison of the fracture mode with the experimental results for sample B4.

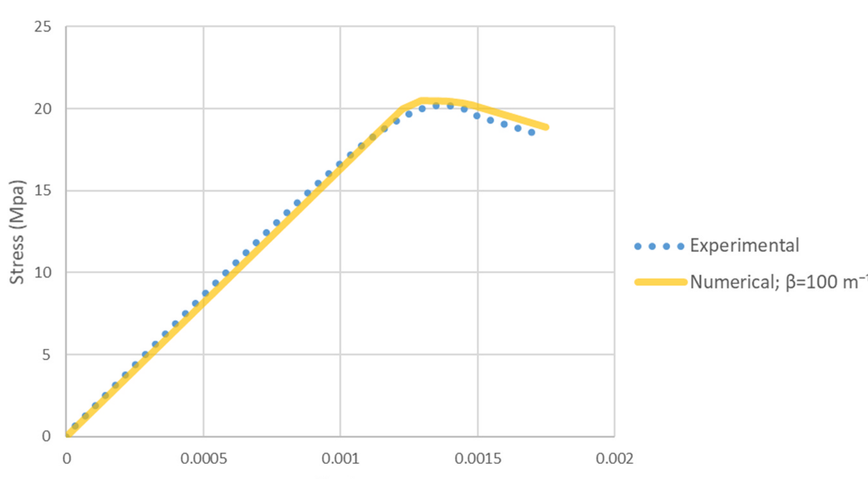

Fig. 9. Average stress–strain curve for sample B4.

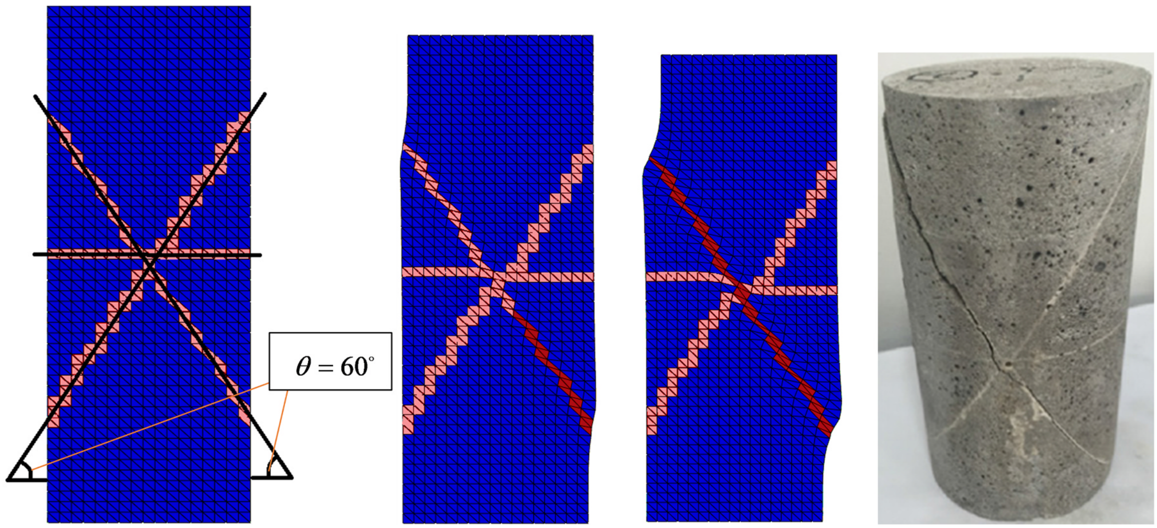

Fig. 10. Comparison of the fracture mode with the experimental results for sample C1.

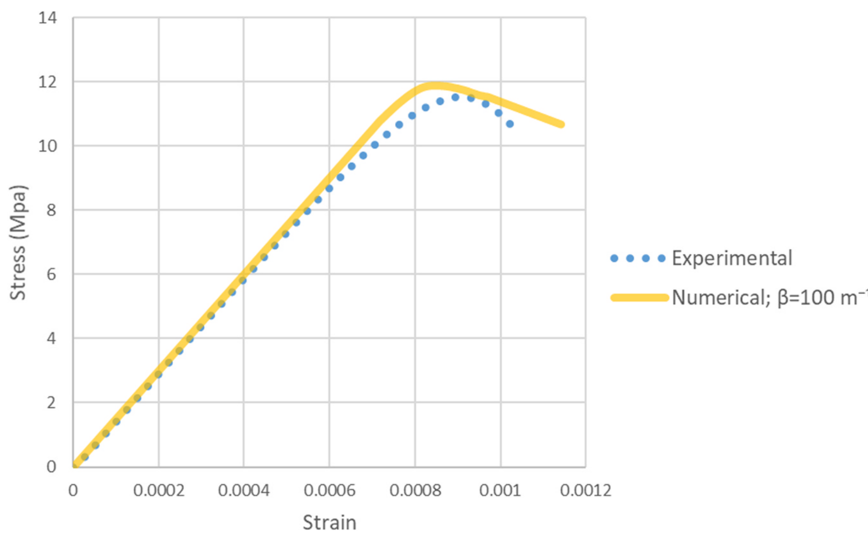

Fig. 11. Average stress–strain curve for sample C1.

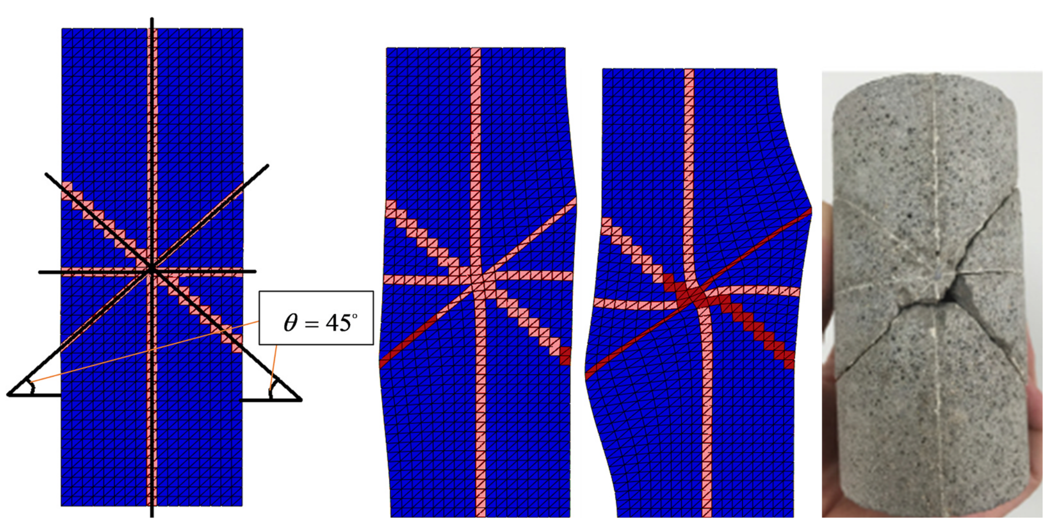

Fig. 12. Comparison of the fracture mode with the experimental results for sample D1.

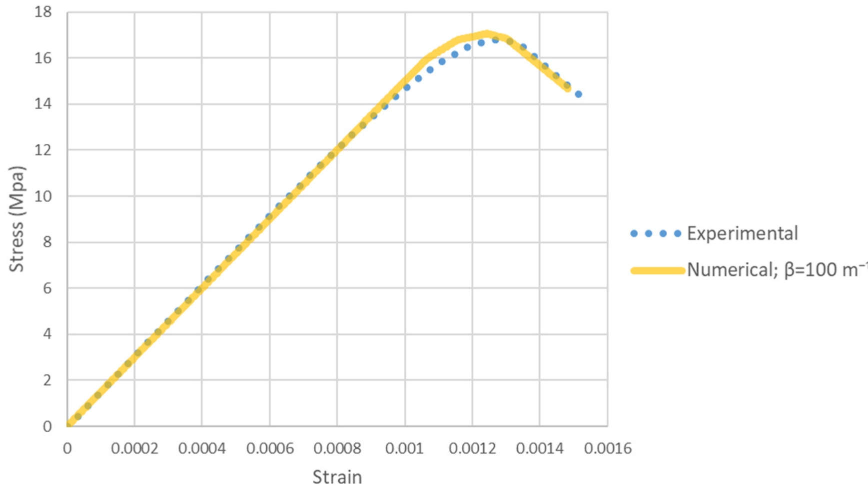

Fig. 13. Average stress–strain curve for sample D1.

3.3. Numerical simulation for sample B4

This example deals with a case involving the presence of two pre-existing cracks, both of them at 45° dip angles with respect to horizontal. Fig. 8 depicts the predicted failure mode. In this case, both fractures are engaged and there is no onset of additional macro-cracking. In the experiment, the loss of stability is also associated with mobilization of sliding along both of the pre-existing faults. Fig. 9 shows the average stress-strain characteristic for the sample. In this case, again, the predicted ultimate load and the post-critical slope are fairly consistent with the experimental data.

3.4. Numerical simulation for sample C1

In this example there are three pre-existing joints, one horizontal and two with 60° dip angle with respect to horizontal. Given the geometry, again a symmetric fracture mode is expected involving sliding along the inclined joints, as the horizontal fracture is not activated here. An asymmetric propagation mode, which was observed experimentally, can be enforced by introducing an inhomogeneity along one of the orientations; in this case, along the joint oriented at the clockwise 60° dip. The numerical results are shown in Figs. 10 and 11. Both, the fracture pattern as well as the average stress-strain response, Fig. 11, are in a very close agreement with the experimental data.

3.5. Numerical simulation for sample D1

In the last example given here, that deals with sample D1, the specimen has four pre-existing fractures; one horizontal, one vertical and two with 45° dip angle with respect to horizontal. In this case, owing to cracks geometry, one would again expect a symmetric fracture mode that involves sliding along the inclined planes. However, in view of the inhomogeneity of the sample, only one orientation gets fully activated. In order to simulate this fracture mode, two imperfections are introduced; a stronger one along the fracture orientation that is predominant in the experiment, and a weaker one along the other conjugate direction. The results, given in Figs. 12 and 13, show a fair agreement with the experimental data. It should be noted that the presence of imperfections affects only the evolution of fracture mode and has virtually no impact on the value of ultimate load.

4. Final remarks

The existing finite element approaches with strong discontinuities (XFEM and EFEM) consist of enriching the (continuous) displacement modes of the standard finite elements with displacement jumps that capture the physical discontinuity. This is done either via element enrichment or nodal enrichment. In both these approaches the discontinuity is embedded within the finite element. The present methodology is also *an embedded discontinuity approach*; however, the discontinuity is accounted for via the constitutive relation by invoking averaging within the referential volume adjacent to the macrocrack. This leads to an improved computational efficiency as, in this case, a standard FE framework can be employed without the need for any additional nodal variables or enrichments. The formulation requires the information on properties of both constituents (i.e. the intact material and the interface) and the 'characteristic dimension' that is uniquely defined.

The results of numerical simulations demonstrate that the framework employed here is capable of predicting complex fracture modes that may emerge in the context of progressive deformation in jointed rock masses. In this case, the existence of pre-defined fractures is often associated with the onset and propagation of new fractures that needs to be properly accounted for.

It is evident from the results that the presence of pre-existing cracks, as well as their orientation, has a profound effect on the value of the compressive strength of the sample. Apparently, the lowest strength is associated with dip angles in the range of 60^0. At the same time, the elastoplastic strain-softening characteristics for the interface material affect the stiffness characteristics, in particular the value of the post-critical modulus.

References

1. Bobet A. *Fracture Coalescence in Rock Materials: Experimental Observations and Numerical Predictions [Ph.D. thesis]*. Cambridge, Massachusetts: MIT; 1997.
2. Dyskin AV, Sahouryeh E, Jewell RJ, Joer H, Ustinov KB. Influence of shape and locations of initial 3-D cracks on their growth in uniaxial compression. *Eng Fract Mech.* 2003;70(15):2115–2136.
3. Li YP, Chen LZ, Wang YH. Experimental research on pre-cracked marble under compression. *Int J Solids Struct.* 2005;42(9–10):2505–2516.
4. Park CH, Bobet A. Crack initiation, propagation and coalescence from frictional flaws in uniaxial compression. *Eng Fract Mech.* 2010;77(14):2727–2748.
5. Cao P, Liu T, Pu C, Lin H. Crack propagation and coalescence of brittle rock-like specimens with pre-existing cracks in compression. *Eng Geol.* 2015;187:113–121.
6. Sagong M, Bobet A. Coalescence of multiple flaws in a rock-model material in uniaxial compression. *Int J Rock Mech Min Sci.* 2002;39(2):229–241.
7. Bobet A, Einstein HH. Fracture coalescence in rock-type materials under uniaxial and biaxial compression. *Int J Rock Mech Min Sci.* 1998;35(7):863–888.
8. Shen B, Stephansson O, Einstein HH, Ghahrcman B. Coalescence of fractures under shear stresses in experiments. *Environ Eng.* 1995;100:5975–5990.
9. Lajtai EZ. Brittle fracture in compression. *Int J Fract.* 1974;10(4):525–536.
10. Wong LNY, Einstein HH. Crack coalescence in molded gypsum and carrara marble: part 1. Macroscopic observations and interpretation. *Rock Mech Rock Eng.* 2009;42(3):475–511.
11. Nilson AH. Nonlinear analysis of reinforced concrete by the finite element method. *ACI J.* 1968;65(9):757–766.

12. Ngo D, Scordelis AC. Finite element analysis of reinforced concrete beams. *ACI J.* 1967;64(3):152–163.
13. Rashid YR. Ultimate strength analysis of prestressed concrete pressure vessels. *Nucl Eng Des.* 1968;7(4):334–344.
14. Pietruszczak S, Mroz Z. Finite element analysis of deformation of strain-softening materials. *Int J Numer Methods Eng.* 1981;17(3):327–334.
15. Pietruszczak S. On homogeneous and localized deformation in water-infiltrated soils. *Int J Damage Mech.* 1999;8(3):233–253.
16. Ingraffea AR, Hueze FE. Finite element models for rock fracture mechanics. *Int J Numer Anal Methods.* 1980;4:25–43.
17. Zhang XP, Wong LNY. Crack initiation, propagation and coalescence in rock-like material containing two flaws: a numerical study based on bonded-particle model approach. *Rock Mech Rock Eng.* 2013;46(5):1001–1021.
18. Tang CA, Kou SQ. Crack propagation and coalescence in brittle materials under compression. *Eng Fract Mech.* 1998;61(3–4):311–324.
19. Haghighat E, Pietruszczak S. On modeling of discrete propagation of localized damage in cohesive-frictional materials. *Int J Numer Anal Methods Geomech.* 2015;39:1774–1790.
20. Zaouter T, Lasseux D, Prat M. Gas slip flow in a fracture: local Reynolds equation and upscaled macroscopic model. *J Fluid Mech.* 2018;837:413–442.
21. Liu J, Sun S, Yue L, Wei J, Wu J. Mechanical and failure characteristics of rock-like material with multiple crossed joint sets under uniaxial compression. *Adv Mech Eng.* 2017;9(7) [168781401770871].
22. Moallemi S, Pietruszczak S. Analysis of localized fracture in 3D reinforced concrete structures using volume averaging technique. *Finite Elem Anal Des.* 2017;125(1):41–52.
23. Grasselli G. *Shear Strength of Rock Joints Based on Quantified Surface Description [Ph.D. thesis].* Ecole Polytechnique Federale de Lausanne; 2001.

Biomechanics and Modeling in Mechanobiology
https://doi.org/10.1007/s10237-020-01319-2

ORIGINAL PAPER

Experimental and analytical study of anisotropic strength properties of bovine cortical bone

H. Mohammadi[1] · S. Pietruszczak[1]

Received: 26 August 2019 / Accepted: 24 February 2020

Abstract
This paper is focused on specification of conditions at failure in bovine cortical bone. Both experimental and analytical studies are conducted. The experimental part includes a series of novel direct shear tests which examine the sensitivity of shear strength to the applied normal stress for different orientations of the sample microstructure. These experiments are supplemented by standard axial compression and tension tests in order to define and quantify a general form of failure criterion. The analytical part examines two different methodologies, viz. critical plane approach and microstructure tensor approach, for defining the anisotropic strength criterion. A procedure for identification of material parameters is outlined which is based on the results of the performed material tests.

Keywords Cortical bone · Anisotropic failure criterion · Bone fracture · Critical plane approach · Microstructure tensor

1 Introduction

Bone tissues, both cortical and trabecular, have complex heterogeneous microstructure which results in an inherent anisotropy in mechanical properties at a macroscale (cf. Martin et al. 2016). Over the last few decades, extensive experimental testing has been conducted to examine those properties. For the trabecular bone, there are intrinsic difficulties in getting consistent quantitative results (Odgaard and Linde 1991; Keaveny et al. 1997). This stems from the fact that the trabecular tissue has high porosity and its microstructure is very inhomogeneous, i.e. varies significantly with the anatomic location. In view of this, the results strongly depend on the size of the sample as well as its orientation relative to the loading direction. The stiffness and strength properties are typically assessed by conducting uniaxial compression tests. However, more comprehensive testing programs, incorporating torsion and multi-axial compression, have also been carried out (Rincón-Kohli and Zysset 2009).

For the cortical bone, the literature on specification of its mechanical properties is more exhaustive, which is due to the fact that this tissue plays a primary role in bearing the physiological and other types of loads. The reported experimental programs involved various loading conditions and included both monotonic and cyclic tests (Zdero 2017). The earliest comprehensive work is perhaps that of Reilly and Burstein (1975), who performed a series of uniaxial tension, uniaxial compression and torsion tests on bovine (with both plexiform and Haversian structure), and human bone samples. The main focus there was on examining the anisotropic nature of properties. The nonlinear effects in uniaxial compression and tension, including development of permanent deformation and cyclic degradation of stiffness, were studied by Nyman et al. (2009). The authors conducted both static and creep tests and demonstrated that the response in compression is associated with larger dissipation of energy and higher stress relaxation than that in tension. A somewhat similar study, focused on development of irreversible (plastic) deformation under cyclic loading in tension, compression, and shear, was conducted by Winwood et al. (2006). The primary objective was the assessment of fatigue life of specimens tested under a prescribed constant stress amplitude. An extension of this work was the subsequent study reported by Zioupos, Gresle and Winwood (2007) who examined the relation between fatigue strength and the bone tissue microstructure, including factors such as age and bone density.

It is interesting to note that the behavior involving shear has been typically assessed by indirect approach that

✉ S. Pietruszczak
pietrusz@mcmaster.ca

[1] McMaster University, Hamilton, ON, Canada

employed tests on structural elements. In experiments conducted by Winwood et al. (2006), notched beam specimens were tested under the vertical load that produced zero bending moment across the notch. In the work reported by Saha (1977), the shear was induced by applying tensile axial load on elongated specimens with asymmetric double notch. A similar double notched specimens were also used by Dong et al. (2013); in the latter case, however, the shear configuration involved testing inclined samples under compressive axial load. All the shear tests mentioned above involved human cortical bone and addressed the issues of strength anisotropy, creep, and/or plastic deformations. While the conclusions reached there are valuable, the interpretation of these tests may be open to question as they, in fact, represent the boundary value problems rather than material tests. A similar concern may be raised in the context of torsional tests on prismatic bars (cf. Park and Lakes 1986). It seems that the only type of *material* tests carried out so far to examine the shear characteristics are the pure shear tests performed by Turner et al. (2001). The latter examined both the strength anisotropy and the effects of fatigue in human cortical bone.

In terms of constitutive modeling of compact bone, one of the first attempts was a simple lower and upper bound assessment of elastic moduli based on mechanics of composite materials (Piekarski 1973). Later, several micromechanical approaches have been pursued for the evaluation of elastic properties and ultimate axial stress. Examples include a model of mineralized collagen fibrils developed by Jäger and Fratzl (2000), or its extension related to unconstrained biological optimization with respect to fracture strength of mineral crystals (Gao et al. 2003). Such formulations, although rigorous, have not been verified and/or applied in the context of structural analysis of whole bones. At the macro-level, the cortical bone tissue is typically idealized as elastic–brittle. Here, the response in the elastic range is usually described using standard Hooke's law for transversely isotropic material. More advanced representations include Cosserat (micropolar) elasticity (Park and Lakes 1986) as well as the Biot's framework of poroelasticity (cf. Cowin 1999). The brittle behavior of cortical bone is perceived as being associated with localized deformation (macrocracking) and has been modeled using volume averaging of discontinuous fields in the vicinity of the crack (Pietruszczak and Gdela 2010).

In terms of specification of conditions at failure, the majority of research effort has been directed at the description of the onset of fracture in *trabecular* bone. Examples here involve the works of Tsai and Wu (1971), Cowin (1986) and Pietruszczak et al. (1999). Tsai and Wu (1971) criterion is an extension of the orthotropic criterion formulated by Hill (1950) which employs an invariant form of a quadratic function of stress components and takes into account the difference in strength in compression and tension regime. This criterion has been employed, with varying degree of success, not only for the trabecular (Fenech and Keaveny 1999) but also for cortical bone (Hayes and Wright 1977; Cowin 1979). Later, Cowin (1986) developed a modified version of Tsai and Wu criterion that incorporates the notion of fabric tensor. Both the above mentioned criteria incorporate a large number of material functions/parameters and are independent of the third stress invariant, which plays an important role in the mechanics of porous media. The latter issue was addressed in the formulation of Pietruszczak et al. (1999) which also introduced a specific fabric measure related to a spatial distribution of void space. More recently, a comprehensive experimental and analytical study was conducted on multi-axial response of trabecular bone and analyzed with a fabric-based generalized Hill criterion (Rincón-Kohli and Zysset 2009). In general, the primary difficulty with describing the conditions at failure in trabecular tissue is the fact that the architecture of trabeculae strongly depends on anatomic location so that the fabric descriptors remain affected by the size of the selected elementary volume. This is in contrast to cortical bone where the principal material axes can be defined a priori based on the geometry of the cortical shell. For *cortical* bone, the most common approaches for defining the conditions of failure involve implementation of strain-based criteria that are largely empirical. Such criteria identify the onset of fracture with critical values of principal strain magnitudes (Niebur et al. 2000) or the strain energy density (Ulrich et al. 1999; Pistoia et al. 2002). In this regard, there is a need for a more general approach, which is rigorous and experimentally verifiable.

This work is focused on the assessment of conditions at failure in bovine cortical bone. The experimental part of this research includes a series of novel direct shear tests which examine the sensitivity of strength to the applied normal stress for different orientations of the sample microstructure. The results of experimental tests are used to formulate and verify the performance of anisotropic failure criteria that incorporate two conceptually different frameworks in which the strength characteristics are linked with material microstructure. In the next section, the details of the experimental program are provided followed by an analytical part dealing with identification of material parameters and verification of the proposed criteria. The last section provides a discussion on the results and final conclusions.

2 Methods and results

Four whole femur bones from one bovine specimen were acquired at a local butcher shop. The slaughter age was within the range of 6–12 months, but no precise information was available. All bones were wrapped in a plastic bag and kept frozen. Prior to sample preparation, the bones were removed from the freezer, thawed at the room temperature, and sprayed with phosphate-buffered saline (PBS) to prevent dehydration. In order to extract the samples, two larger segments (of approx. 5 cm) were first cut with a band saw from the mid-diaphysis region. Subsequently, using the machine tools the square prisms of average dimensions $5 \times 5 \times 11$ mm (for direct shear and compression testing) and dog-bone shape (for tension) samples were prepared. The specimens were cut in different anatomical directions. The vertical (longitudinal) samples were extracted along the diaphysis, while the horizontal (transverse) ones were perpendicular to it. In the shear tests, a number of intermediate orientations between 0° and 90° were employed. Before testing, the samples were soaked in PBS for 4 h at the room temperature. Also, during the machining process the samples were continuously irrigated. The compression and tension tests were conducted using an Instron (model 5967) machine, while the shear tests were performed in a modified direct shear apparatus. All tests were displacement-controlled with a constant loading rate of 0.03 mm/s.

2.1 Micro-CT scan of a specimen

Prior to mechanical testing, a CT scan was conducted on one of the prism-shaped samples. The scan was performed using a high-resolution desktop X-ray micro-CT system Bruker Skyscan 1172 with a variable X-ray energy range from 20 to 100 kV. The pixel size was 6.6 µm, rotation step 0.4°, and a 0.5 mm AL filter was used to get images at 66 kV, 149 µA. Four frames were averaged for each image to maximize the signal to noise ratio with 8 s. integration time. The objective of the µCT scan was to ensure that the sample preparation, which involved cutting and smoothing of the specimen, did not induce any visible damage. Figure 1 shows various cross-sectional views together with a 3D reconstructed image of the sample before its testing. The dark spots appearing in those images represent Haversian canals and/or osteon boundaries. Based on a visual inspection, there is no evidence of macrocracks growth and coalescence inside as well as at the external surfaces of the sample. This indicates that the internal structure has not been significantly altered in the process of sample preparation.

2.2 Direct shear tests

The direct shear tests are typically used for assessing the mechanical competence of geomaterials (soils or rocks) as well as cohesive-frictional interfaces. They have not been employed before in the context of biomechanical testing. Their primary purpose is to determine the shear strength under different values of the applied normal stress and to identify the strength parameters appearing in Coulomb criterion (viz. friction angle and cohesion). A schematic picture of a direct shear box is shown in Fig. 2 (cf. Das 2002). The box is split horizontally at mid-height, and the tests are conducted by applying the horizontal (shear) displacement to the upper part under a constant vertical load. The mechanical characteristics are typically presented in terms of a relation between the shear traction and displacement discontinuity along the failure plane, which is constrained to remain horizontal. In the present study, a series of direct shear tests was performed in order to demonstrate that for a cortical tissue, the conditions at failure, in compression regime, are not significantly affected by the confining pressure. This aspect has not been explicitly addressed in the literature before.

The *soil* samples commonly tested in a direct shear device are shaped like flat disks or flat square prisms; the sample diameter/width is typically 5–10 cm, and the thickness is within a range of 2–2.5 cm. The samples of *cortical bone* were square prisms with an average cross-sectional area of 5×5 mm; therefore, the mold had to be refined to accommodate these dimensions. In addition, given the small size of the cortical bone samples and the surface irregularities, a thin layer (approx. 1 mm) of fine sand was placed at the top and bottom surfaces. This was to ensure that the vertical load is applied to the sample in a uniform way.

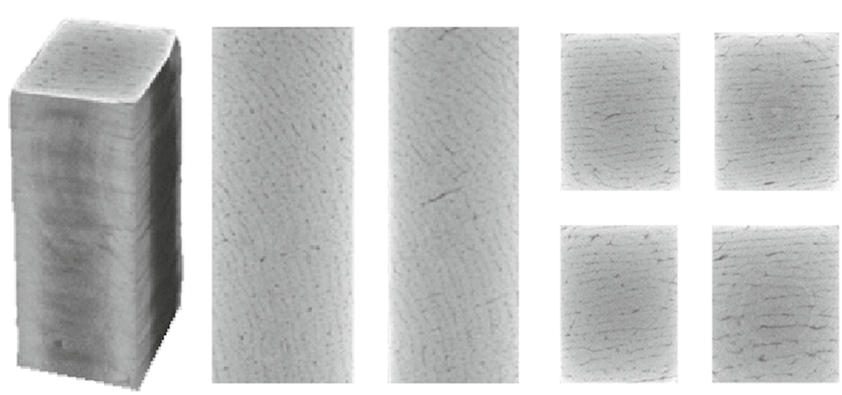

Fig. 1 Micro CT scan results for one of the samples. Left: 3D reconstructed sample; center: vertical sections from the 3D model in two perpendicular directions; right: view of four different cross sections of the sample

Fig. 2 Schematic diagram of a standard direct shear test set up

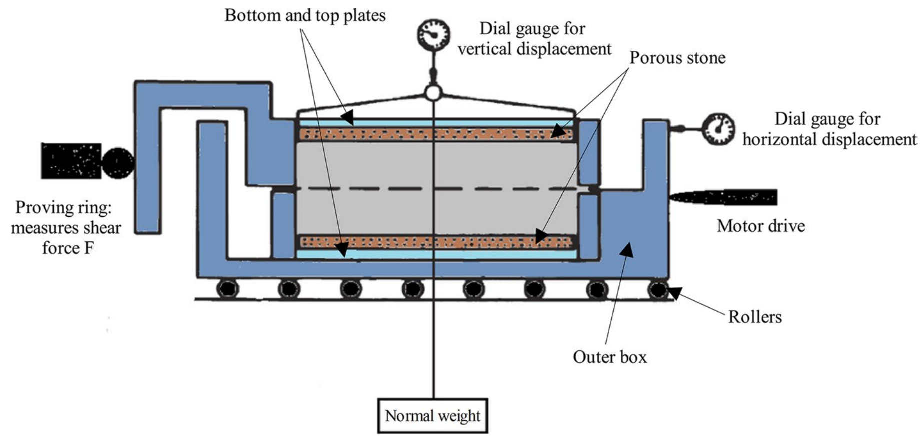

2.3 Results of direct shear tests

The tests were carried out on sets of four differently oriented samples, i.e. $\beta = 0°$, 30°, 60°, 90°, where $\beta = 90°$ refers to longitudinal (vertical) direction. At least, three tests were conducted for each assigned value of normal load. Altogether, the results of 45 shear tests on samples taken from *the same bovine specimen* are reported here. This is in addition to a series of preliminary tests that were carried out on different bovine samples in order to assess the efficiency of the modifications to the shear device itself and the consistency of the results.

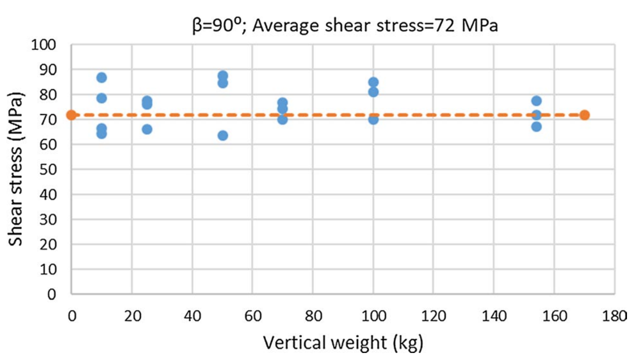

Fig. 3 Variation of ultimate shear stress versus vertical weight; longitudinal samples, $\beta = 90°$

The experimental results for longitudinal samples ($\beta = 90°$) are presented in Fig. 3, which shows the values of shear strength for a range of predetermined vertical loads. It is evident that, in this case, there is virtually no reduction in average shear strength with the decrease in the value of normal stress. This is in contrast to frictional materials which exhibit a strong sensitivity in this respect. Thus, the conditions at failure within the range of *compressive* normal stress may perceived as *pressure-independent*. It should be noted that during the tests, the normal stress was applied by placing weights on a loading frame. The cross-sectional area of each sample over which this load was applied was slightly different, thereby resulting in different normal stress. Therefore, for the clarity of presentation, the results in Fig. 3 are shown as an explicit function of selected weights. It ought to be pointed out that since the shear strength is virtually constant, the actual value of normal stress is of no direct significance here. Figure 4 shows the plots for the remaining orientations, viz. $\beta = 0°$, 30°, 60°. The results are presented here in terms of the average values and the standard deviation, and it is evident again that the shear strength is orientation-dependent. The latter observation is highlighted in Fig. 5 which shows a combined graph of average shear strength versus normal stress for different values of β.

It is noted that the cortical bone, both human and bovine, has a low porosity of approx. 3–7%. This range is typical for different types of microstructures that include plexiform,

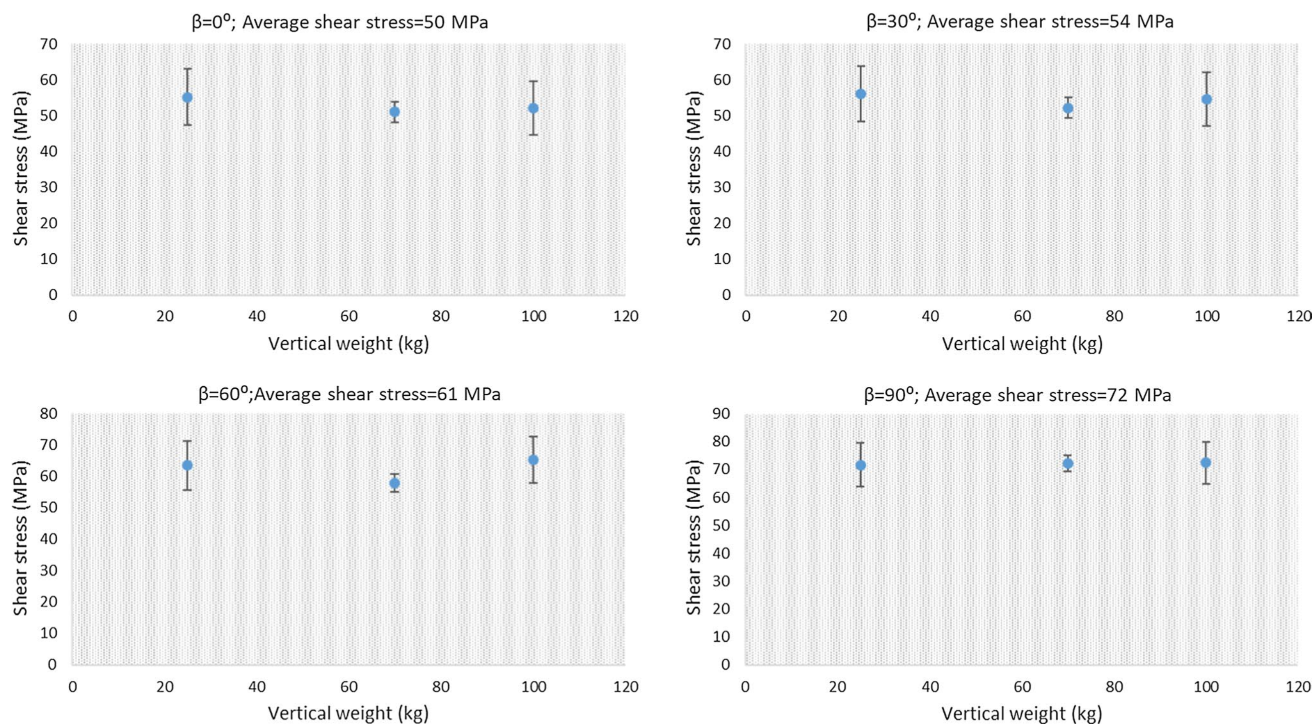

Fig. 4 Shear strength (viz. average values and standard deviation) versus vertical weight for different values of β

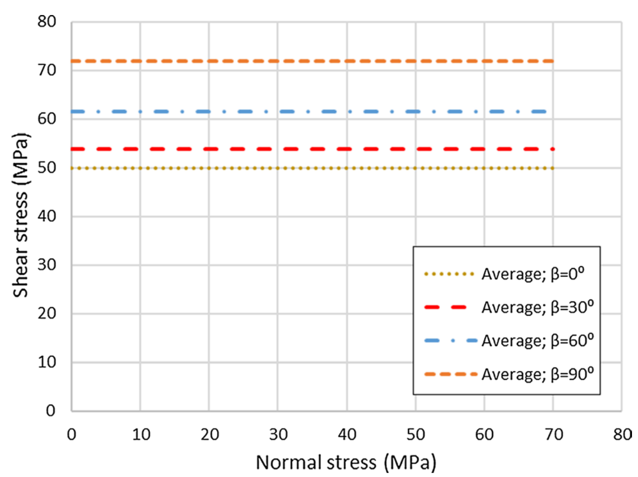

Fig. 5 Average shear strength versus normal stress for different values of β within the range 0°–90°

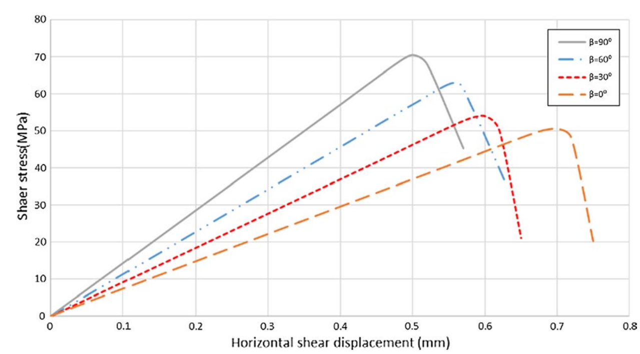

Fig. 6 Shear stress versus horizontal displacement curves (vertical weight 25 kg)

Haversian (osteonal) and/or mixed. The low porosity is the primary reason behind the lack of sensitivity of shear strength to the value of normal stress. Thus, although the strength itself will be affected by the microstructural arrangement of the bone tissue, the qualitative conclusion regarding its insensitivity to the normal stress is likely to hold for human cortical bone as well.

Finally, Fig. 6 shows a set of average shear stress—horizontal displacement characteristics at a constant vertical weight (25 kg) for different orientations of the sample. It is evident that once the ultimate strength is reached the response becomes unstable (strain-softening), which is associated with sliding along the horizontal rapture surface.

2.4 Results of axial compression/tension tests

The uniaxial compression tests were carried out in conventional Instron testing machine. Only longitudinal and transverse samples were tested ($\beta = 90°$ and $0°$, respectively). The reason for this was twofold. The first was the limitation on the number of samples, and second, the fact that for inclined samples, the end platens impose kinematic constraints that may render the results not to be fully reliable. The latter stems from the inherent anisotropy which implies that inclined specimens will tend to distort under vertical load. For each orientation, a series of three tests was performed and the average axial stress–strain response is shown in Fig. 7. Both the strength and stiffness are orientation-dependent, and the behavior becomes unstable after the peak. It is noted that the results of these tests were used primarily for the verification of the proposed failure criterion, as discussed in the next section.

The uniaxial tension tests were carried out again on longitudinal and transverse samples only. The corresponding average axial stress–strain characteristics are presented in Fig. 8. It is evident that the behavior is elastic–brittle with strength strongly dependent on the orientation of the sample. It is noted here that the tensile strength is significantly lower than the compressive one which indicates that the failure criterion in tension regime is likely to have a different functional form from that in compression.

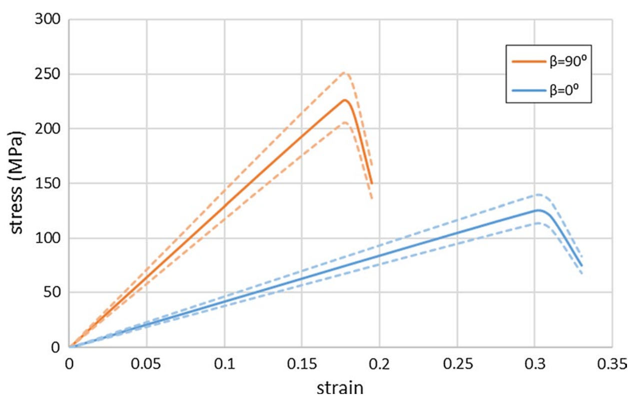

Fig. 7 Stress–strain curves for uniaxial compression tests

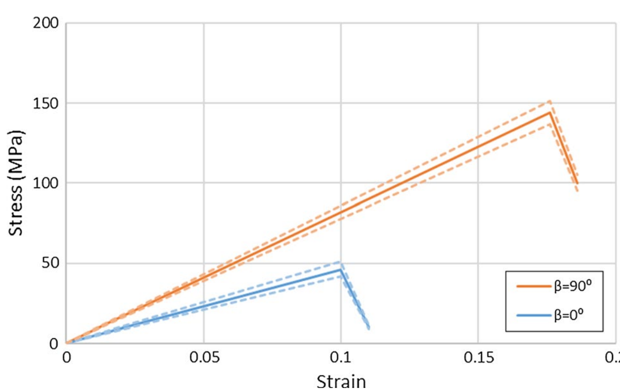

Fig. 8 Stress–strain curves for axial tension tests

3 Failure criterion for the cortical bone

As evidenced by the experimental data presented in the previous section, the shear stress at failure along a pre-defined plane does not appear to be significantly affected by the value of normal stress. At the same time, the strength varies with the orientation of the sample. Given this evidence, it is postulated that the conditions at failure in compression regime may be approximated by invoking Tresca or von Mises-like criterion enhanced to account for inherent anisotropy in properties. Furthermore, the ultimate stress in axial tension is significantly lower than that in compression, indicating that Rankin type of cutoff condition is required to limit the strength in the tensile region. In what follows, two alternative approaches are outlined, in which the strength characteristics are linked with material microstructure. In particular, the critical plane approach and the framework incorporating the notion of anisotropy parameter, as proposed by Pietruszczak and Mroz (2001), are employed. For both these methodologies, the material functions are specified from the experimental tests conducted here and the general procedure for their identification is outlined.

3.1 Critical plane approach for Tresca criterion

In the critical plane methodology, the failure function F is defined in terms of traction vector $\boldsymbol{t}$ acting on a plane with the unit normal $\boldsymbol{n}$. Thus,

$$F = f(\boldsymbol{t}) - c(\boldsymbol{n}) \tag{1}$$

where c is an orientation-dependent strength parameter. The failure takes place when $F = 0$, i.e. $f = c$, while the orientation of the failure plane is obtained by solving a constrained optimization problem, i.e.

$$\max_{\boldsymbol{n}} (f(\boldsymbol{t}) - c(\boldsymbol{n})) = 0; \quad c = c_0\big(1 + \boldsymbol{n}\cdot\boldsymbol{\Omega}\cdot\boldsymbol{n} + b_1(\boldsymbol{n}\cdot\boldsymbol{\Omega}\cdot\boldsymbol{n})^2 + b_2(\boldsymbol{n}\cdot\boldsymbol{\Omega}\cdot\boldsymbol{n})^3 + \cdots\big) \tag{2}$$

Here, b's are the coefficients of approximation, while $\boldsymbol{\Omega}$ is a symmetric traceless tensor which is collinear with the principal material axes and whose eigenvalues define the bias in the spatial distribution of $c(\boldsymbol{n})$. It should be noted that for a transversely isotropic material, there is only one independent eigenvalue of $\boldsymbol{\Omega}$ as $\mathrm{tr}\,\boldsymbol{\Omega} = 0$.

For Tresca criterion, only the tangential component of traction vector is employed and c is identified with the ultimate shear stress. Thus, in this case, there is

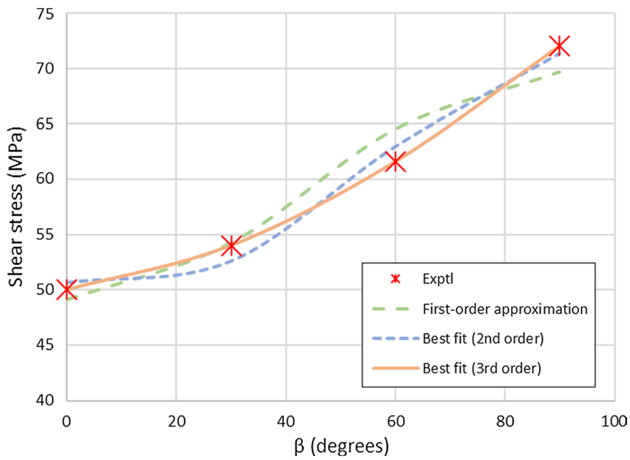

Fig. 9 Experimental results of direct shear tests and their best-fit approximations

$$F = |\boldsymbol{n} \cdot \boldsymbol{\sigma} \cdot \boldsymbol{s}| - c(\boldsymbol{n}); \quad \boldsymbol{n} \cdot \boldsymbol{s} = 0; \quad \max_{\boldsymbol{n},\boldsymbol{s}} F = 0 \tag{3}$$

where $\boldsymbol{s}$ is a unit vector orthogonal to $\boldsymbol{n}$. The corresponding Lagrangian function takes the form

$$G = |\boldsymbol{n} \cdot \boldsymbol{\sigma} \cdot \boldsymbol{s}| - c_0\big(1 + \boldsymbol{n} \cdot \boldsymbol{\Omega} \cdot \boldsymbol{n} + b_1(\boldsymbol{n} \cdot \boldsymbol{\Omega} \cdot \boldsymbol{n})^2 + b_2(\boldsymbol{n} \cdot \boldsymbol{\Omega} \cdot \boldsymbol{n})^3 + \cdots\big) - \lambda_1(\boldsymbol{n} \cdot \boldsymbol{n} - 1) - \lambda_2 \boldsymbol{n} \cdot \boldsymbol{s} - \lambda_3(\boldsymbol{s} \cdot \boldsymbol{s} - 1) \tag{4}$$

Imposing now the stationary conditions with respect to $\boldsymbol{n}$, $\boldsymbol{s}$ and λ's, the onset of localization and the orientation of the failure plane may be determined.

Table 1 Parameters for critical plane approach based on best-fit approximation

Parameters	First-order approximation	Second-order approximation	Third-order approximation
C_0	62.83	60.634	59.511
Ω_1	0.1093	0.1448	0.1211
b_1		1.496	4.5017
b_2			12.7837

Table 2 Comparison of experimental results with numerical predictions for uniaxial compression

	σ_1 (MPa)	
β	0°	90°
Experimental	120	225
Linear approximation	109	200
Second-order approximation	112	219
Third-order approximation	119	224

The function $c(\boldsymbol{n})$ can be identified from the results of direct shear tests reported in the previous section. Figure 9 shows the variation of average shear strength with the orientation of the sample (i.e., angle β). The best-fit approximations of orders 1–3, incorporating transverse isotropy in representation (3), are also depicted in this figure while the corresponding coefficients of approximation are given in Table 1. It is noted that here the strength is monotonically increasing with β and, as a result of it, a lower-order approximation (2–3) appears to be sufficiently accurate.

In order to verify the performance of this framework, the response under uniaxial compression is considered. Assuming again the transverse isotropy and referring the problem to the principal material axes, Eqs. (2)–(4) lead to

$$F = \left|\frac{1}{2}\sigma \sin 2\alpha\right| - c_0\left\{1 + \Omega_1\xi + b_1\Omega_1^2\xi^2 + b_2\Omega_1^3\xi^3\right\}; \quad \xi = 1 - 3\cos^2(\alpha - \beta) \tag{5}$$

$$\frac{\mathrm{d}F}{\mathrm{d}\alpha} = S\sigma\cos 2\alpha - c_0\Omega_1\frac{\mathrm{d}\xi}{\mathrm{d}\alpha} - 2c_0b_1\Omega_1^2\xi\frac{\mathrm{d}\xi}{\mathrm{d}\alpha} - 3c_0b_2\Omega_1^3\xi^2\frac{\mathrm{d}\xi}{\mathrm{d}\alpha}$$
$$\frac{\mathrm{d}\xi}{\mathrm{d}\alpha} = 3\sin 2(\alpha - \beta); \; S = \mathrm{sign}(\sigma\cos 2\alpha) \tag{6}$$

where α is the orientation of the failure plane with respect to the horizontal. By imposing $F = 0 \wedge \frac{\mathrm{d}F}{\mathrm{d}\alpha} = 0$ and solving the above set of equations, both the ultimate stress intensity σ and the orientation of the localization plane can be defined. Table 2 shows the comparison of computed values with the experimental results for different orders of approximation. It is evident that in this case, the higher order approximations give more accurate results. As mentioned earlier, the experimental data are restricted here to orientations of $\beta = 0$, 90° in view of limitations of the testing program.

3.2 Critical plane approach for tension cut-off

The simplest approximation here is the Rankine cut-off criterion which postulates that the failure occurs when a critical value of normal stress is reached along the failure plane. Thus,

$$F = |\boldsymbol{n} \cdot \boldsymbol{\sigma} \cdot \boldsymbol{n}| - f_t(\boldsymbol{n}); \quad \max_{\boldsymbol{n}} F = 0;$$
$$f_t = f_{to}\big(1 + \boldsymbol{n} \cdot \boldsymbol{\Omega} \cdot \boldsymbol{n} + d_1(\boldsymbol{n} \cdot \boldsymbol{\Omega} \cdot \boldsymbol{n})^2 + d_2(\boldsymbol{n} \cdot \boldsymbol{\Omega} \cdot \boldsymbol{n})^3 + \cdots\big) \tag{7}$$

Here, the function $f_t(\boldsymbol{n})$ defines the ultimate strength for tension perpendicular to the set of planes with unit normal $\boldsymbol{n}$, d's are the coefficients of approximation while $\boldsymbol{\Omega}$ describes the distribution bias. In the special case when $d_1 = d_2 = \cdots = 0$, the remaining parameters can be related to strength along the principal material axes. Assuming again that the material is transversely isotropic and denoting the tensile resistance along the direction of lamellae and perpendicular to it as $f_{t\parallel}, f_{t\perp}$, respectively, the representation (7) yields

$$f_{to} = \left(f_{t\parallel} + 2f_{t\perp}\right)/3;\ \Omega_1 = \frac{f_{t\perp}}{f_{to}} - 1 \tag{8}$$

The values of the above parameters can be obtained *implicitly* from the results of uniaxial tension tests on horizontal/vertical specimens, as provided in the previous section. For the linear approximation (i.e. $d_1 = d_2 = \cdots = 0$), the functional form (7) can be expressed, after some algebraic manipulations, as

$$F = \sigma \cos^2 \alpha - f_{to}\left(1 + \Omega_1 \chi\right) = 0;\ \ \chi = 1 - 3\cos^2(\alpha - \beta) \tag{9}$$

and

$$\frac{dF}{d\alpha} = -\sigma \sin 2\alpha - f_{to}\Omega_1 \frac{d\chi}{d\alpha} = 0;\ \frac{d\chi}{d\alpha} = 3\sin 2(\alpha - \beta) \tag{10}$$

Note that the experimental data for uniaxial tension at $\beta = 0$, 90°, provide the ultimate stress σ as well as the corresponding orientation of the failure plane α. The latter, for tests conducted in the principal material axes, is orthogonal to the direction of maximum principal stress. Given this information, Eqs. (9) and (10) can be solved for the two respective unknowns, i.e. f_{to}, Ω_1. For the data reported in the previous section, there is $f_{to} = 111.33$ MPa; $\Omega_1 = 0.293$.

Another way of defining the tensile strength criterion would be a bi-linear approximation, whereby the failure function in tension regime is assumed as

$$F = f_t|\boldsymbol{n} \cdot \boldsymbol{\sigma} \cdot \boldsymbol{s}| + c|\boldsymbol{n} \cdot \boldsymbol{\sigma} \cdot \boldsymbol{n}| - c f_t;\quad \max_{\boldsymbol{n},\boldsymbol{s}} F = 0 \tag{11}$$

The above representation has a similar functional form to that of Coulomb criterion, while the material functions $c = c(\boldsymbol{n})$ and $f_t = f_t(\boldsymbol{n})$ are defined viz. Equations (2) and (7), respectively.

3.3 Microstructure tensor approach for Tresca criterion

An alternative approach to specifying the conditions at failure involves incorporation of an anisotropy parameter which depends on relative orientation of principal stress and material axes (Pietruszczak and Mroz 2001). Following this methodology, any isotropic failure criterion can be extended to the case of anisotropy by assuming

$$F(\boldsymbol{\sigma}) = F(I_1, J_2, J_3, \eta) \tag{12}$$

where $I_1 = \mathrm{tr}(\boldsymbol{\sigma})$, J_2, J_3 are the basic invariants of the stress deviator and η is a scalar anisotropy parameter. The latter may be expressed in the form

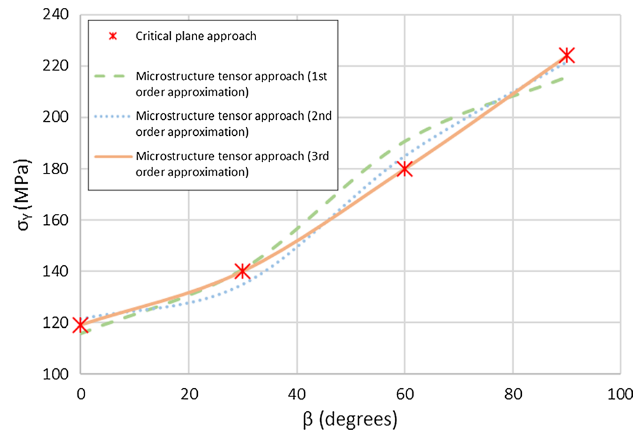

Fig. 10 Variation of compressive strength based on approximation (17); 'virtual data' generated from critical plane approach

$$\eta = \eta_0(1 + \boldsymbol{l} \cdot \boldsymbol{A} \cdot \boldsymbol{l} + a_1(\boldsymbol{l} \cdot \boldsymbol{A} \cdot \boldsymbol{l})^2 + a_2(\boldsymbol{l} \cdot \boldsymbol{A} \cdot \boldsymbol{l})^3 + \cdots) \tag{13}$$

Here, $\boldsymbol{l}$ represents a versor along a generalized *loading vector* $\boldsymbol{L}$, that is defined as

$$\boldsymbol{L} = L_\alpha \boldsymbol{e}^{(\alpha)};\quad L_\alpha^2 = \boldsymbol{t}^{(\alpha)} \cdot \boldsymbol{t}^{(\alpha)} = (\boldsymbol{e}^{(\alpha)} \cdot \boldsymbol{\sigma}) \cdot (\boldsymbol{e}^{(\alpha)} \cdot \boldsymbol{\sigma}) \tag{14}$$

where $\boldsymbol{e}^{(\alpha)}$, $\alpha = 1, 2, 3$, are the base vectors which specify the direction of preferred material axes. Thus, the components of $\boldsymbol{L}$ represent the magnitudes of tractions $\boldsymbol{t}$ acting on planes normal to the principal material axes. The latter are defined by the eigenvectors of the operator $\boldsymbol{A}$, which is a traceless second-order tensor.

Using the functional form (12), the Tresca criterion may be expressed as (cf. Pietruszczak 2010)

$$F = \sqrt{3}\bar{\sigma} - g(\theta)\sigma_c = 0; g(\theta) = \frac{3}{2\sqrt{3}\cos\theta} \tag{15}$$

where $\bar{\sigma} = \sqrt{J_2}$ and θ is the Lode's angle, i.e. $\theta = -\sin^{-1}(\sqrt{27/4}J_3 \big/ J_2^{3/2})/3$. Note that the scalar parameter η, appearing in Eq. (12), is identified here with ultimate strength in axial compression σ_c, i.e. $\eta = \sigma_c$, so that for an anisotropic material

$$\sigma_c = \hat{\sigma}_c(1 + \boldsymbol{l} \cdot \boldsymbol{A} \cdot \boldsymbol{l} + a_1(\boldsymbol{l} \cdot \boldsymbol{A} \cdot \boldsymbol{l})^2 + a_2(\boldsymbol{l} \cdot \boldsymbol{A} \cdot \boldsymbol{l})^3 + \cdots) \tag{16}$$

The coefficients appearing in the approximation (16) can be defined from the results of axial compression tests conducted at different orientations of the sample (i.e., angle β). In this case, Eq. (16) reduces to

$$\sigma_c = \hat{\sigma}_c(1 + A_1\chi + a_1A_1^2\chi^2 + a_2A_1^3\chi^3 + \cdots); \chi = 1 - 3\cos^2\beta \tag{17}$$

As mentioned before, the experimental tests performed in this work were restricted to $\beta = 0°, 90°$. This was due to the fact that for intermediate orientations, the results of axial compression are not reliable as the presence of rigid platens constraints the sample distortion which typically occurs in an anisotropic material. This, in turn, leads to a non-uniform stress state within the sample which affects the value of ultimate strength. Given this limitation, the identification procedure is illustrated here by invoking a set of 'virtual data' generated using critical plane approach with the values of parameters given in Table 1 (3rd order approximation). The results of best-fit approximation for σ_c involving representation (17) are provided in Fig. 10. The 3rd order approximation, which is the most accurate here, yields the following values of coefficients

$$\hat{\sigma}_c = 170.43,\ A_1 = 0.2018,\ a_1 = 2.0491,\ a_2 = 3.5258$$

Finally, it should be noted that for $g(\theta) = \text{const.}$, Eq. (15) reduces to von Mises criterion that can also be employed as an alternative representation.

3.4 Microstructure tensor approach for tension cut-off

In the tension regime, the Rankine cutoff criterion can be expressed as

$$F = \sigma_1 - \sigma_t(\boldsymbol{l}) = \left(2/\sqrt{3}\right)\bar{\sigma}\sin(\theta + 2/3\,\pi) + 1/3\,I_1 - \sigma_t(\boldsymbol{l}) = 0 \tag{18}$$

where $\sigma_t(\boldsymbol{l})$ is the axial tensile strength, which is expressed in the functional form analogous to Eq. (16). Again, this function can be identified explicitly from the results of direct tension tests at different orientations of the sample. Given the fact that no comprehensive experimental data are available here in that respect, again the set of 'virtual data' was generated using the critical plane methodology. Figure 11 shows the results of simulations for critical plane approach that correspond to the set of parameters $f_{to} = 111.33\,\text{MPa}$; $\Omega_1 = 0.293$, as identified in Sect. 3.2, together with the best-fit approximation for $\sigma_t(\boldsymbol{l})$ employing a linear form, i.e.

$$\sigma_t = \hat{\sigma}_t(1 + A_1\chi);\ \chi = 1 - 3\cos^2\beta \tag{19}$$

The coefficients of this approximation are $\hat{\sigma}_t = 110.07$, $A_1 = 0.2737$.

It should be noted that the tensile strength criterion could again be expressed in an alternative form that incorporates a bi-linear approximation in $(\bar{\sigma}, I_1)$-space, analogous to that suggested in Sect. 3.2, Eq. (11).

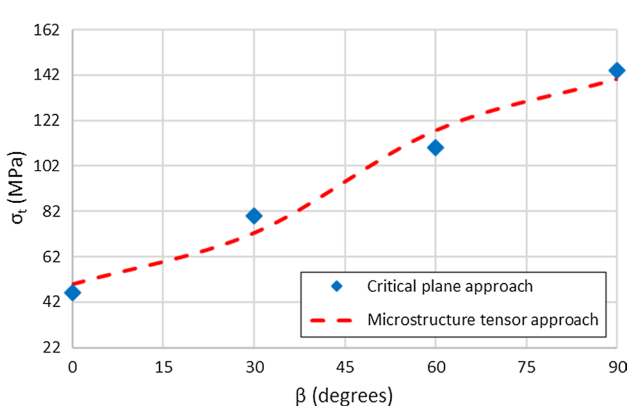

Fig. 11 Variation of tensile strength based on approximation (19); 'virtual data' from critical plane approach

4 Discussion

As mentioned earlier in this paper, the shear strength of cortical bone is typically assessed by indirect approach that employs structural tests, such as 3-point bending, torsion, and/or tension of specimens with asymmetric double notch. The interpretation of the results of these tests is not straightforward as they represent, in fact, *boundary value problems*. A more accurate and appropriate way of assessing the strength is to employ the *material tests*. The idea of a material test is that the boundary conditions remain uniform and the representative elementary volume of the sample is sufficiently large, in relation to its microstructure, so that the stress state may be perceived as homogeneous, in a statistical sense, at the macroscale.

The experimental work presented here involved a series of material tests which were conducted using a direct shear device. The primary objective was to examine the sensitivity of shear strength to the applied normal stress for different orientations of the sample microstructure. The results indicate that the strength is virtually independent of the value of normal stress. Thus, the conditions at failure *in compression regime* are not affected by the first stress invariant; however, they depend on the orientation of the material triad in relation to the principal stress system. The reason for the pressure insensitivity of strength appears to be twofold. First, the low porosity of material; and second, the presence of fluid phase, i.e. generation of excess fluid pressure which limits the compressibility of pore space. The results also indicated that *in tension regime,* the strength of the material is significantly reduced and it is also affected by the orientation of the sample.

It should be emphasized that the tests conducted here involved a bovine cortical bone. From a structural point of view, bovine and human cortical bones have different growing rates, and consequently different microstructure. The human bone has a Haversian architecture, while bovine can be either plexiform or mixed with a Haversian system composed of lamellae, depending on the age and anatomic location. The difference in microstructure will inevitably affect the quantitative aspects of the results. At the same time, however, both types of tissue have low porosity and contain interstitial fluid, so that it is likely that the qualitative conclusions reached here will hold for a human cortical bone as well.

The failure criteria advocated in this work are phenomenological in nature; however, the formulation is enhanced by incorporating some information on microstructure (viz. tensorial operators $\boldsymbol{\Omega}$ or $\boldsymbol{A}$, whose eigenvectors define the principal material axes). This is in contrast to commonly used anisotropic criteria, like those of Hill (Hill 1950; Garcia et al. 2009) and/or Tsai–Wu (1971), which do not incorporate any explicit fabric measures. Hill criterion defines the conditions at failure in terms of all independent components of stress tensor referred to the principal material system. As a result, it requires a series of pure shear tests, in addition to direct compression/tension tests, performed in the principal material configuration. The former cannot be easily conducted on bone tissues. In addition to difficulties associated with identification of parameters, Hill criterion postulates that the strength in compression and tension regime is the same. This is not true for cortical tissue, since not only the strength itself, but also its spatial variation is significantly different in compression and tension. Furthermore, Hill criterion implies that the variation of strength follows the classical rules of transformation, which is clearly not the case here (see, for example, Fig. 11). Tsai–Wu criterion, which is an extension of Hill's work, is also expressed in a quadratic form which incorporates all independent stress components. In this formulation, the strength in tension and compression regime is different; the general form, however, is pressure-dependent. The latter contradicts the findings in this work, so that applicability of this criterion to cortical bone may be questioned. The Tsai–Wu failure function employs 12 material parameters (compared to 6 for Hill criterion) and the spatial variation of compressive and tensile strength is implied again by standard transformation rules.

An alternative approach to formulation of anisotropic criteria is the representation that explicitly incorporates a tensorial measure of fabric (cf. Boehler and Sawczuk 1977; Cowin 1986). In this case, the general framework employs all ten independent invariants of the both stress and fabric tensors, together with a large number of associated material parameters that cannot be explicitly identified. The approach followed in this paper is a pragmatic compromise between the two methodologies mentioned above. It incorporates independent material functions governing the spatial distribution of strength parameters and the constants involved are the coefficients of approximation (not the intrinsic material parameters). The latter can be directly identified from standard material tests, as explained in Sect. 3. It should be noted that both critical plane and the microstructure tensor approach are two alternative methodologies and either one can be used in the numerical analysis. Our objective was not to give preference to any of them, but to explain the differences in the procedure for identification of material parameters and to assess their performance.

In summary, the main novel aspects in this work include the following: (1) the use of a direct shear test in assessing the conditions at failure in a cortical bone; (2) the first, to authors' knowledge, experimental evidence that in compression regime, the failure criterion is virtually independent of the first stress invariant; (3) experimental evidence that the directional dependence of strength properties does not follow standard transformation rules and requires a more elaborate representation. Finally, it should be stressed that the conclusions reached here in relation to the mathematical form of the proposed failure criterion require further experimental verification. In particular, their validity needs to be assessed in other multi-axial loading configurations.

References

Boehler JP, Sawczuk A (1977) On yielding of oriented solids. Acta Mech 27:185–206

Cowin SC (1979) On the strength anlsotropy of bone and wood. J Appl Mech 46:832–838

Cowin SC (1986) Fabric dependence of an anisotropic strength criterion. Mech Mater 5:251–260

Cowin SC (1999) Bone poroelasticity. J Biomech 32:217–238

Das BM (2002) Soil mechanics laboratory manual, 6th edn. Oxford University Press, New York

Dong XN, Luo Q, Wang X (2013) Progressive post-yield behavior of human cortical bone in shear. Bone 53(1):1–5. https://doi.org/10.1016/j.bone.2012.11.029

Fenech CM, Keaveny TM (1999) A cellular solid criterion for predicting the axial-shear failure properties of bovine trabecular bone. J Biomech Eng 121:414–422

Gao H et al (2003) Materials become insensitive to flaws at nanoscale: lessons from nature. Proc Natl Acad Sci U S A 100(10):5597–5600

Garcia D, Zysset PK, Charlebois M, Curnier A (2009) A three-dimensional elastic plastic damage constitutive law for bone tissue. Biomech Model Mechanobiol 8:149–165

Hayes WC, Wright TM (1977) An empiricl strength theory for compact bone. Fracture 3:1173–1179

Hill R (1950) The mathematical theory of plasticity. Oxford University Press, London

Jäger I, Fratzl P (2000) Mineralized collagen fibrils: a mechanical model with a staggered arrangement of mineral particles. Biophys J 79(4):1737–1746

Keaveny TM et al (1997) Systematic and random errors in compression testing of trabecular bone. J Orthop Res 15(1):101–110

Martin RB, Burr DB, Sharkey NA, Fyhrie DP (2016) Skeletal tissue mechanics, 2nd edn. Springer, New York

Niebur GL et al (2000) High-resolution finite element models with tissue strength asymmetry accurately predict failure of trabecular Bone. J Biomech 33:1575–1583

Nyman JS, Leng H, Dong XN, Wang X (2009) Differences in the mechanical behavior of cortical bone between compression and tension when subjected to progressive loading. J Mech Behav

Biomed Mater 2(6):613–619. https://doi.org/10.1016/j.jmbbm.2008.11.008
Odgaard A, Linde F (1991) The underestimation of Young's modulus in compressive testing of cancellous bone specimens. J Biomech 24(8):691–698
Park HC, Lakes RS (1986) Cosserat micromechanics of human bone: strain redistribution by a hydration sensitive constituent. J Biomech Eng 19(5):385–397
Piekarski K (1973) Analysis of bone as a composite material. Int J Eng Sci 11(6):557–565
Pietruszczak S (2010) Fundamentals of plasticity in geomechanics. CRC Press, Boca Raton
Pietruszczak S, Gdela K (2010) Inelastic analysis of fracture propagation in distal radius. J Appl Mech 77:1–10
Pietruszczak S, Mroz Z (2001) On failure criteria for anisotropic cohesive-frictional materials. Int J Numer Anal Meth Geomech 25(5):509–524
Pietruszczak S, Inglis D, Pande GN (1999) A fabric-dependent fracture criterion for bone. J Biomech 32(10):1071–1079
Pistoia W et al (2002) Estimation of distal radius failure load with micro-finite element analysis models based on three-dimensional peripheral quantitative computed tomography images. Bone 30(6):842–848
Reilly DT, Burstein AH (1975) The elastic and ultimate properties of compact bone tissue. J Biomech 8(6):393–405
Rincón-Kohli L, Zysset PK (2009) Multi-axial mechanical properties of human trabecular bone. Biomech Model Mechanobiol 8(3):195–208
Saha S (1977) Longitudinal shear properties of human compact bone and its constituents, and the associated failure mechanisms. J Material Sci 12:1798–1806
Tsai SW, Wu EM (1971) A general theory of strength for anisotropic materials. J Compos Mater 5(1):58–80
Turner CH, Wang T, Burr DB (2001) Shear strength and fatigue properties of human cortical bone determined from pure shear tests. Calcif Tissue Int 69:373–378
Ulrich D, Rietbergen BV, Laib A, Rüegsegger P (1999) Load transfer analysis of the distal radius from in-vivo high resolution CT imaging. J Biomech 32:821–828
Winwood K et al (2006) Strain patterns during tensile, compressive, and shear fatigue of human cortical bone and implications for bone biomechanics. J Biomed Mater Res 79(2):289–297
Zdero R (2017) Experimental methods in orthopaedic biomechanics. Academic Press, London
Zioupos P, Gresle M, Winwood K (2007) Fatigue strength of human cortical bone: age, physical, and material heterogeneity effects. J Biomed Mater Res 86:627–636

(Submitted to Journal of Biomechanical Engineering)

Numerical analysis of hip fracture due to a sideways fall

Hojjat Mohammadi
Department of Civil Engineering, McMaster University, Hamilton, Ontario, Canada
mohamh1@mcmaster.ca
Stanislaw Pietruszczak[1]
Department of Civil Engineering, McMaster University, Hamilton, Ontario, Canada
pietrusz@mcmaster.ca
Cheryl E. Quenneville
Department of Mechanical Engineering, McMaster University, Hamilton, Ontario, Canada
School of Biomedical Engineering, McMaster University, Hamilton, Ontario, Canada
quennev@mcmaster.ca

ABSTRACT

The primary purpose of this paper is to outline a methodology for evaluating the likelihood of cortical bone fracture in the proximal femur in the event of a sideways fall. The approach includes conducting finite element (FE) analysis in which the cortical bone is treated as an anisotropic material and the admissibility of the stress field is validated both in tension and compression regime. In assessing the onset of fracture, two methodologies are used, viz. Critical Plane approach and the Microstructure Tensor approach. The former is employed in the tension regime, while the latter governs the conditions at failure in compression. The propagation of localized damage is modeled using a constitutive law with embedded discontinuity (CLED). In this approach the localized deformation is described by a homogenization procedure in which the average properties of cortical tissue intercepted by a macrocrack are established. The key material properties governing the conditions at failure are specified from a series of independent material tests that are conducted on cortical bone samples tested at different orientation relative to the loading direction. The numerical analysis deals with simulations of tests involving the sideways fall and the results are compared with the experimental data. This includes both the evolution of fracture and the local load-displacement characteristics.

Keywords: *Cortical bone, Failure criterion, Inherent anisotropy, Microstructure tensor approach, Finite element analysis*

[1] pietrusz@mcmaster.ca

INTRODUCTION

Fracture of the hip is one of the most pervasive fractures in the world that causes morbidity and loss of life [1]. In isolated cases these have been attributed to contraction of the muscles [2], although clinically it has been reported that hip fractures are most frequently caused by sideways falls from heights [3]. In order to address the underlying mechanical conditions, numerous experiments have been conducted incorporating various loading configurations, e.g. those representative of single leg stance [4], standing [5], sideways fall [6], and/or impact [7-9].

Because of the diversity of bone tissue microstructure and variations in geometry of human femoral bone among the population, subject-specific finite element (FE) models based on quantitative computed tomography (QCT) have been developed. These were employed in both single-leg stance [10-14] as well as sideways fall conditions [15-19]. Most of these models were validated against mechanical tests conducted ex-vivo and some were found to produce better predictions of femoral strength and/or fracture load than the assessment based on BMD measurements [12, 17]. It should be pointed out though that the solutions often involved a trial-and-error adjustment of the material parameters in order to enhance the predictive abilities of the models in relation to the experimental data. In most cases, no independent experimental studies were conducted to identify the actual mechanical properties of the bone tissue.

Early approaches to assess the hip fracture risk by means of FE analysis date back to 1990's. The research employed data from quantitative computed tomography (QCT) images to construct the proximal femur models, while the analysis itself was conducted in the linear elastic range [20] as well as in a nonlinear range [21]. In the latter case, a constitutive relation for concrete was employed to model the trabecular tissue, whereas for the cortical bone a simple bi-linear law was used. For both approaches, the selection of material parameters was rather speculative, and the results showed a significant discrepancy in assessment of fracture load as compared to experimental tests. At the same time, however, the analysis itself provided a rational platform for further research.

More recent numerical studies on femoral fracture focused on prediction of crack initiation and propagation. Different methodologies have been employed including the use of cohesive zone elements [22, 23], homogenized voxel models at continuum level [15], continuum damage mechanics approaches involving deletion of cracked elements [24, 25], as well as the models incorporating the Extended Finite Element (XFE) method. All these mathematical frameworks, except for XFE method, do not employ any non-local dimension, thereby resulting in a pathological mesh-dependency of the solution. The XFE approach has attracted increasing attention in numerical analysis of tensile fracture in biomaterials. Examples of application of XFE include the work of Marco et al. [26, 27] dealing with the assessment of the accuracy of XFE models in evaluating the early stages of the crack propagation as well as in tracing of the crack path in a heterogeneous human femoral bone. The XFE framework incorporates a local enrichment of the shape functions in order to account for the presence of discontinuity within the FE mesh. This requires employment of additional degrees of freedom as well as special integration techniques, which significantly deters the numerical efficiency. This is particularly evident in the context of 3D simulations involving biomechanical applications. In addition, the XFE packages in commercial software, such as Abaqus, are prone to divergence when dealing with fracture patterns involving propagation of long single cracks and/or multiple intersecting cracks [27, 28].

In terms of modeling of mechanical properties of cortical tissue, one of the first attempts was a basic lower and upper bound assessment of elastic moduli [29]. Subsequently, several micro as well as macro-mechanically based approaches involving assessment of elastic properties as well as the ultimate axial strength have been employed [30, 31]. More sophisticated approaches include Cosserat elasticity [32], the poroelasticity framework of Biot (cf. [33]), and/or the adoption of a homogenization technique (viz. volume averaging) for the cortical bone tissue intercepted by a fractured zone [34].

In terms of specification of the conditions at failure for trabecular bone, the attempts include the works of Tsai and Wu [35], Cowin [36], Pietruszczak et al. [37]. Tsai and Wu [35] criterion was implemented, with varying degrees of success, not only for the trabecular [38] but also for the cortical bone [39, 40]. In a follow up development, Cowin [36] formulated a modified version of this criterion by incorporating the notion of fabric tensor. More recently, a comprehensive experimental and analytical study on multiaxial response of trabecular bone was conducted by Rincón-Kohli and Zysset [41]. In general, it is difficult to define the conditions at failure in trabecular tissue since the architecture of trabeculae is highly dependent on the anatomic location so that the macroscale description is strongly affected by the size of elementary volume considered.

The present research is focused on modeling of femur fracture triggered by a low speed sideways fall. These types of fractures are most common in older adults [3, 42]. The cortical tissue is assumed to be anisotropic and its strength is considered as orientation dependent. This is in contrast to several other approaches that often ignore the notion of material anisotropy (e.g. [13, 14, 43]). In assessing the onset of fracture, two different frameworks are used, viz. Critical Plane and the Microstructure Tensor approach [44]. The former is employed in the tension domain, while the latter governs the conditions at failure in compression regime. The evolution of crack path is modeled using a constitutive law with embedded discontinuity (CLED). In this approach the localized deformation is described by a volume averaging procedure in which the equivalent properties of cortical tissue intercepted by a macrocrack are established (cf. [45]). The advantages of this approach are twofold. First, the numerical results are mesh-independent, and second, the formulation could be used within the standard FEM platform rather than XFE, which is computationally more efficient. In the next section, the mathematical framework is outlined together with description of the experimental program aimed at specification of material parameters. Subsequently, the results of 3D numerical analysis are discussed and compared with the experimental data. This includes both the evolution of fracture pattern within the femur and the macroscopic load-displacement characteristics.

MATERIAL AND METHODS

The numerical component of this work involves simulation of one of the ex-vivo experimental tests reported in a recent paper by Jazinizadeh et al. [9]. The test was conducted on a proximal femur from a female donor (age 73) with total BMD of 759 mg/cm2. The specimen was tested to failure in a load configuration representative of a sideways fall and the details of this and other similar static/dynamic tests are provided in the original reference. The main focus here is on a verification of the mathematical framework for assessing the onset and propagation of localized damage within the cortical tissue, as outlined in section 2.1. below. In order to provide a quantitative validation, additional experimental tests have been conducted on small samples of cortical tissue extracted from the entire femur immediately after the fracture test. This enabled identification of the primary material parameters governing the strength anisotropy, which were subsequently employed in FE analysis. In what follows, the formulation of the problem is reviewed first, followed by the description of experimental tests.

Mathematical formulation

The onset of localized deformation, associated with the formation of macrocracks, is modeled here using the anisotropic fracture criteria for cortical tissue as recently proposed and validated by Mohammadi and Pietruszczak [46]. Those involve a Rankine-type of tension criterion formulated within the framework of critical plane approach, as well as an enhanced Tresca criterion incorporating the notion of a microstructure tensor. The latter governs the conditions at failure in compression regime. For tensile failure, the orientation of macrocrack is defined as a constrained optimization problem while the propagation of damage is described by a homogenization procedure invoking a constitutive law with embedded discontinuity (cf. [34]). The proposed approach renders the results that are mesh independent and can uniquely answer the question whether the failure mode associated with a sideways fall involves tensile and/or shear induced fracture.

Critical plane approach in tension regime

The cortical tissue is perceived as a transversely isotropic material and the failure function is formulated in terms of normal component of traction acting on a plane with unit normal $\boldsymbol{n}$. The tensile strength itself is assumed to be orientation-dependent and the spatial bias in its distribution is described by employing a traceless second-order tensor $\boldsymbol{\Omega}$. The failure function is defined as (c.f. [44])

$$F = t^n(\mathbf{n}) - f_t(\mathbf{n}); \;\; \max_{\mathbf{n}} F = 0; \;\; f_t = \hat{f}_t(1 + \mathbf{n}\cdot\mathbf{\Omega}\cdot\mathbf{n}) \tag{1}$$

where, $f_t(\boldsymbol{n})$ is the strength for tension along $\boldsymbol{n}$ and $\hat{f}_t$ is a material constant. By employing the Lagrange multiplier method, the orientation of the localization plane can be obtained by solving the following eigenvalue problem

$$\left(\mathbf{B}-\lambda\boldsymbol{\delta}\right)\cdot\mathbf{n}=0;\ \mathbf{B}=\boldsymbol{\sigma}-c_0\boldsymbol{\Omega} \tag{2}$$

where $\boldsymbol{\delta}$ is the Kronecker delta. Given the orientation **n**, the value of failure function in eq. (1) can be checked. Apparently, F<0 is indicative of elastic response, while for F=0 the initiation of fracture takes place.

Enhanced anisotropic Tresca criterion in compression regime

It was recently demonstrated that, in compression regime, the conditions at failure in cortical tissue may be viewed as pressure-independent [46]. In this case, the initiation of fracture may be described in terms of Tresca criterion enhanced by introducing the notion of a microstructure tensor. The latter allows to relate the tissue strength to the orientation of principal stress axes relative to material directions.

The failure function defining the Tresca criterion in the presence of anisotropy can be expressed in terms of stress invariants as (cf. [47])

$$F=\sqrt{3}\bar{\sigma}-\frac{3}{2\sqrt{3}\cos\theta}f_c=0;\quad f_c=\hat{f}_c(1+\boldsymbol{l}\cdot\boldsymbol{A}\cdot\boldsymbol{l}+b_1\left(\boldsymbol{l}\cdot\boldsymbol{A}\cdot\boldsymbol{l}\right)^2+b_2\left(\boldsymbol{l}\cdot\boldsymbol{A}\cdot\boldsymbol{l}\right)^3+...) \tag{3}$$

Here, θ is the Lode's angle, $\bar{\sigma}=\sqrt{J_2}$, where J_2 is the stress deviator, and f_c is the axial compressive strength, which is assumed to be orientation-dependent. The latter is described in terms of a polynomial representation, viz. second equation in (3), in which $\boldsymbol{A}$ is a traceless second-order tensor, and $\boldsymbol{l}$ is a unit normal along the loading vector $\boldsymbol{L}$ defined as

$$\boldsymbol{L}=L_i\boldsymbol{e}^{(i)};\quad L_i^2=\boldsymbol{t}^{(i)}\cdot\boldsymbol{t}^{(i)} \tag{4}$$

where $\boldsymbol{e}^{(i)}$, $i=1,2,3$, are the base vectors specifying the preferred principal material axis and $\boldsymbol{t}$ is the traction vector.

It is noted that the material function $f_c(l_i)$ can be identified from axial compression tests performed on differently oriented samples of cortical tissue (cf. [48]). In this case, the functional form of f_c reduces to

$$f_c = \hat{f}_c(1 + A_1\xi + b_1 A_1^{\,2}\xi^2 + b_2 A_1^{\,3}\xi^3 + ...); \quad \xi = 1 - 3\cos^2\alpha \tag{5}$$

where α is the angle between the direction of osteons and that of axial loading.

Volume averaging approach for fractured region

The formulation involves the decomposition of the stress and strain rates within the domain containing a discontinuity into the volume averages associated with the basic constituents; i.e. intact material and fractured region (cf. [45]). Assuming that the thickness of the fractured zone is small compared to other dimensions of the referential volume, there is

$$\dot{\boldsymbol{\sigma}} = \dot{\boldsymbol{\sigma}}^{(0)} + \nu\dot{\boldsymbol{\sigma}}^{(1)}; \ \dot{\boldsymbol{\varepsilon}} = \dot{\boldsymbol{\varepsilon}}^{(0)} + \nu\dot{\boldsymbol{\varepsilon}}^{(1)} \tag{6}$$

Here, ν is the volume fraction of the localization zone, while the superscripts 0,1 refer to material in the intact and the fractured region, respectively. The average strain rate resulting from localized deformation is defined in terms of the dyadic product of the velocity discontinuity, $\dot{\boldsymbol{u}}$, and the unit normal $\boldsymbol{n}$. Thus,

$$\dot{\boldsymbol{\varepsilon}}^{(1)} = \frac{1}{h}(\boldsymbol{n} \otimes \dot{\boldsymbol{u}})^s \tag{7}$$

where h is thickness of the fractured zone, and the superscript (s) refers to the symmetric part of the operator.

The macroscopic response can now be obtained by imposing the continuity of traction $\boldsymbol{t}$ across both regions and writing the governing constitutive relations in an incremental form

$$\dot{\boldsymbol{t}} = \boldsymbol{n} \cdot \boldsymbol{\sigma}^{(0)}; \ \dot{\boldsymbol{\sigma}}^{(0)} = \mathbb{D} : \dot{\boldsymbol{\varepsilon}}^{(0)}; \ \dot{\boldsymbol{t}} = \boldsymbol{K} \cdot \dot{\boldsymbol{u}} \tag{8}$$

where $\mathbb{D}, \boldsymbol{K}$ are the respective tangential stiffness operators. Substituting eqs. (7) and (8) in eq. (6), and performing some algebraic manipulations leads to

$$\dot{\boldsymbol{u}} = \mathbb{L} : \dot{\boldsymbol{\varepsilon}}; \quad \mathbb{L} = \left(\boldsymbol{K} + \chi\left(\boldsymbol{n} \cdot \mathbb{D} \cdot \boldsymbol{n}\right)\right)^{-1} \otimes \boldsymbol{n} : \mathbb{D} \tag{9}$$

where χ is a "characteristic dimension" defined as the ratio of the area of the macrocrack to the considered referential volume. Using the localization law (9), as specified above, the rate form of the governing stress-stain relation may be expressed as

$$\dot{\boldsymbol{\sigma}} = \mathbb{D}\left(\mathbb{I} - \chi \boldsymbol{n} \otimes \mathbb{L}\right) : \dot{\boldsymbol{\varepsilon}} \tag{10}$$

where $\mathbb{I}$ is the fourth order unit tensor.

The implementation of the constitutive relation (10) requires the specification of properties of the intact and fractured material, viz. $\mathbb{D}, \boldsymbol{K}$. The former are considered here as anisotropic elastic (prior to localization), while the latter are assessed using a plasticity based strain-softening framework. For cracks forming in tension regime, the loading criterion is assumed in a simple functional form

$$f = \boldsymbol{t} \cdot \boldsymbol{t} - k^2;\; k = k_0 e^{-\beta\eta};\; \dot{\eta} = \boldsymbol{n} \cdot \dot{\boldsymbol{u}}^p \tag{11}$$

where k_0 is the magnitude of traction at the initiation of localization, η is the plastic part of the normal component of displacement discontinuity (crack opening) and β is a constant that controls the rate of softening. By following a standard plasticity procedure, i.e. satisfying the consistency condition and imposing an associated flow rule, the following expression for the matrix **K** is obtained

$$\boldsymbol{K} = \boldsymbol{K}^e + \boldsymbol{t} \otimes \boldsymbol{t}/H;\; H = 2kk'\left(\boldsymbol{n} \cdot \boldsymbol{t}\right) \tag{12}$$

where $\boldsymbol{K}^e$ is the elastic operator.

Experimental procedure

A clinical CT of the full bone was taken prior to the fracture testing in order to obtain the geometry for the FE simulations. After the fracture test, segments of cortical bone were removed for the material testing. The sample preparation followed the procedure described below.

Immediately after the fracture test, the femur bone was wrapped in a plastic bag and kept frozen at -20ºC. Prior to material testing, the bone was thawed for approximately four hours at room temperature, and two large pieces were removed from the mid-diaphysis. Subsequently, six dog-bone shape samples were prepared (i.e., three for each direction of testing) by using an end mill. A schematic picture of the sample geometry and the actual dimensions are shown in Fig. 1-A. The specimens were cut in longitudinal and transverse directions, with longitudinal samples extracted along the diaphysis, and transverse samples perpendicular to it. During the cutting process, the samples were periodically irrigated with water to prevent dehydration. Once prepared, the specimens were then soaked in phosphate buffered saline (PBS), and later placed again in the freezer until they were tested.

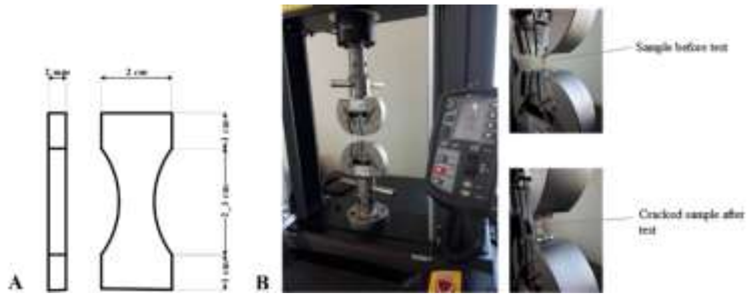

Fig. 1 A) A schematic picture of sample geometry and the actual dimensions; B) The testing machine (Instron, Model 5967); sample in the testing machine before and after the test

Prior to conducting the material tests, a micro CT scan was performed in order to evaluate the integrity of the samples. The scan was done for one of the tested specimens using Bruker Skyscan 1172 (pixel size 6.6 µm, rotation step 0.40, 0.5mm AL filter for getting images at 66 kV, 149 µA.). The objective of the µCT scan was to check whether the sample preparation, which involved cutting and smoothing of the specimen, induced any visible damage resulting in generation of micro and/or macrocracks.

The material testing involved a series of uniaxial tension tests that were required to identify the material parameters employed in the critical plane approach, viz. eq.(1). The testing was performed on longitudinal and transverse samples; all tests were displacement-controlled and involved a constant loading rate of 0.03 mm/sec. The testing was done using an Instron machine (Model 5967), as shown in Fig. 1-B. The grippers of this testing machine were fixed on the wider part of each sample and the specimens were aligned with the center of the load cell.

EXPERIMENTAL AND NUMERICAL RESULTS

In this section the results of experimental tests performed on cortical tissue, as well as numerical simulations involving the femur fracture test are presented. The former include the results of the micro CT scan as well as the stress-strain characteristics obtained in axial tension. Subsequently, the issue of specification of material constants for both critical plane approach and microstructure tensor approach is discussed, followed by the details of FE analysis and the comparison of the results with experimental data.

Experimental results and identification of material parameters

The results of the micro CT scan are depicted in Fig. 2. The figure shows different cross-sectional views, together with the reconstructed 3D image of the sample before the test. The dark spots visible in those images represent Haversian canals and/or osteon boundaries. Based on a visual inspection, there is no evidence of microcracks growth and coalescence inside as well as at the external surfaces of the sample. This indicates that the internal structure has not been significantly altered in the process of sample preparation.

Fig.3 shows the obtained stress-strain characteristics for longitudinal and transverse samples. It is noted that for intermediate orientations the results would not be reliable, as the inclined samples will tend to distort in the presence of anisotropy, which is constrained by the kinematic boundary conditions. The results indicate that both the strength and the stiffness properties are affected by the presence of anisotropy. The strength of longitudinal samples (114±8 MPa) is significantly higher than that of transverse samples (50±3 MPa).

The next aspect of the analysis is the specification of material parameters based on the experimental findings. In order to do so, consider first the tensile strength criterion, eq.(1). According to this equation, for a transversely isotropic material, the expression defining the spatial distribution of $f_t(\boldsymbol{n})$ reduces to

$$f_t = \hat{f}_t \left(1 + \Omega_1 \left(1 - 3\cos^2 \alpha\right)\right) \tag{13}$$

where α is the angle between direction of osteons and the horizontal plane, so that $\alpha = 90^0$ refers to the longitudinal sample. For the simple functional form (13), the approximation coefficients $\hat{f}_t, \Omega_1$ can be defined directly in terms of values of the tensile strength for transverse $f_t^{(tr)}$ and longitudinal $f_t^{(l)}$ samples. Thus

$$\hat{f}_t = \frac{1}{3}\left(f_t^{(tr)} + 2 f_t^{(l)} \right); \quad \Omega_1 = \frac{f_t^{(l)}}{\hat{f}_t} - 1 \tag{14}$$

which for $f_t^{(tr)}$ =50 MPa and $f_t^{(l)}$ =114 MPa yields $\hat{f}_t = 92.67$ MPa; $\Omega_1 = 0.23$.

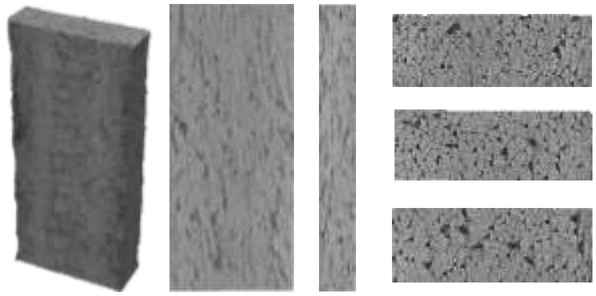

Fig. 2 Micro CT scan of the sample at different sections

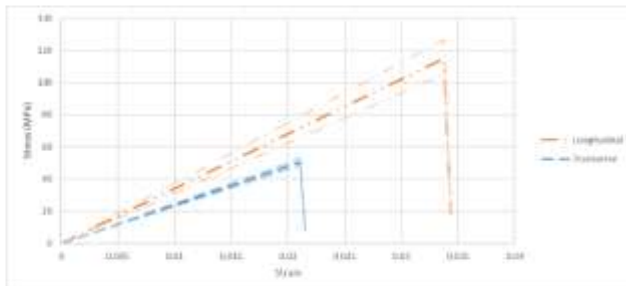

Fig. 3 Stress strain curve for longitudinal and transverse samples (thinner dashed lines are showing the standard deviation)

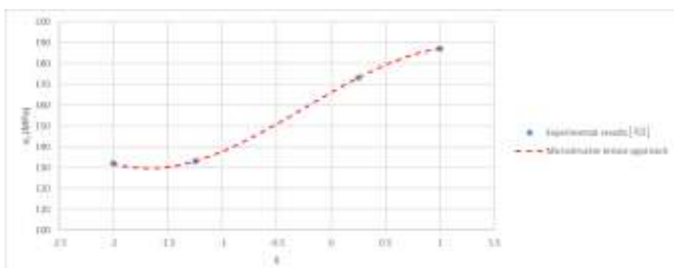

Fig. 4 Spatial distribution of uniaxial compressive strength, including the 3rd order best-fit approximation based on the microstructure tensor approach

In the numerical simulations presented later in this section, the cortical tissue is assumed to be elastic brittle. While the onset of localization in tension regime is described by the anisotropic strength criterion (1), the static admissibility of stress in the compression regime is checked by invoking the failure function (3) which incorporates the notion of microstructure tensor. The identification of this framework requires a series of axial compression tests on differently oriented samples. No such tests have been performed in this work. Instead, the approximation coefficients have been chosen based on some typical values of axial strength of human cortical tissue as reported in the work of Reilly and

Burstein [48]. Fig. 4 shows their experimental data together with the third order best fit approximation based on representation (5). The latter resulted in the following values of coefficients

$$\hat{f}_c = 165.9 \text{ MPa}, \; A_1 = 0.178, \; b_1 = -0.676, \; b_2 = -5.278$$

It is recognized that the values of compressive strength adopted herein may not be very accurate for the cortical tissue tested in this work. It needs to be emphasized, however, that these values are used only to verify the plastic admissiblity of stress field in compression regime. As demonstrated in the following section, the numerical simulations of femur fracture involve damage associated with formation of tensile cracks, as governed by eqs. (11)-(12), while in compression regime the value of F, as defined by eq.(3), remains significantly below zero.

Results of numerical analysis and comparison with experimental data

The geometry of the femoral bone was reconstructed from the CT scan data file, which was obtained prior to fracture testing. Subsequently, the FE mesh employing approx. 76500 four- noded tetrahedral solid elements was generated using Mimics and 3-Matics software and was then imported to a commercial FE solver (Abaqus FEA). Numerical subroutines for integration of constitutive relations presented in Section 2.1 were developed and incorporated in the same commercial package.

The boundary conditions of the problem are shown schematically in Fig. 5. The support #1 was fixed in y-direction and support #2 was fixed in all three directions to prevent translational movement; however, no restrain on rotation was imposed. The gray areas shown in Fig. 5 indicate the PMMA pads, which were used in the experiment to maintain a uniform load. The loading process was displacement-controlled and consisted of applying a quasi-static concentrated load on the greater trochanter to simulate the conditions similar to those employed in the experiment.

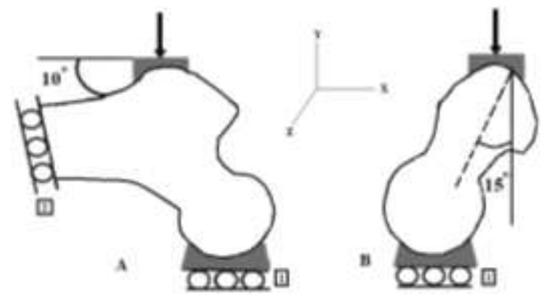

Fig. 5 Schematic diagram of geometry and boundary conditions for simulating the sideways fall

The strength properties of cortical tissue were selected according to the data provided in Section 3.1. The specification of elastic constants for a transversely isotropic material requires, in general, three different tests, i.e. uniaxial tension, uniaxial compression, and torsion [49]. The experimental results obtained in this study were therefore insufficient to identify all five independent parameters. In view of this, the values reported by Krone and Schuster [50] were used, as listed in Table. 1. In this table, the subscript 1 refers to the longitudinal direction, while 2 and 3 are the directions perpendicular to it. It should be pointed out that the stiffness properties obtained in the present study (viz. Fig. 3) are within the range of values reported by Krone and Schuster [50] as well as by other investigators (e.g., [48, 50]).

Table.1 Material parameters adopted in numerical analysis

Cortical bone strength	Please refer to section 3.1
Cortical bone elastic properties[50]	$E_1 = 16000\ MPa$ $E_2 = E_3 = 6300\ MPa$ $G_{12} = G_{13} = 3300\ MPa$ $\upsilon_{12} = \upsilon_{13} = 0.3$ $\upsilon_{23} = 0.45$
Trabecular bone strength[41] Trabecular bone elastic properties[51]	$f_t = 4.0\ MPa$; $f_c = 10.2\ MPa$ $E = 500\ MPa$; $\upsilon = 0.3$
Marcrocrack properties	$k_N = k_T = 1*10^9\ MPa/mm$ $\beta = 150\ m^{-1}$

Trabecular bone has a complex microstructure and its properties highly depend on the anatomical location and the associated geometry of trabeculae. A detailed description of mechanical behaviour of this tissue is beyond the scope of the present study. It needs to be emphasized, however, that the mechanical competence of femur bone is largely governed by the properties and the geometry of the cortical bone. In the numerical simulations presented here, the trabecular tissue was modelled using the properties reported in Kutz [51] and listed in Table 1. Some parametric studies were conducted in order to evaluate the sensitivity of the solution (in particular, the assessment of fracture load) to the value of the elastic modulus.

For both, cortical and cancellous bone, the fracture criteria (1) and (3) governing the onset of macrocracking were employed. The crack propagation was modeled using the constitutive relation defined in Section 2.1.3, i.e. eq. (10). The implementation of this framework requires the values of elastic moduli k_N and k_T for the damaged region, as well as the parameter β, eq.(11), governing the rate of strain softening. All these parameters can, in general, be identified from a direct shear/tension tests along the fracture plane. In this study, however, no experimental data was available in this respect. Therefore, these parameters were selected on a somewhat intuitive basis. The elastic contact moduli were assigned very large values, cf. Table 1, implying that the predominant mechanism for the interface is the irreversible (plastic) deformation. The constant β was initially assigned a value typical for cemented cohesive materials (cf. [52]), i.e. β =150m^{-1}, and a parametric study has been performed to assess its influence on the results of simulations. The orientation of crack in the tension regime was defined by solving the eigenvalue problem (2). There was no evidence of the onset of localized damage in the compression regime, as explained later in this section.

The main results of the numerical analysis are presented in Figs. 6-10. Figs. 6-A and 6-B show the evolution of crack pattern in two different views; anterior and posterior. The regions marked in red show the elements in which the macrocracks form. It should be noted that in the numerical simulations no special algorithm for a discrete crack tracing was employed and, as a results, the cracks appear as smeared over a certain region. The predicted crack pattern is, in general, in a fairly good agreement with the experimental observation. For completeness of the results, Fig. 6-C shows the crack penetration into the trabecular region.

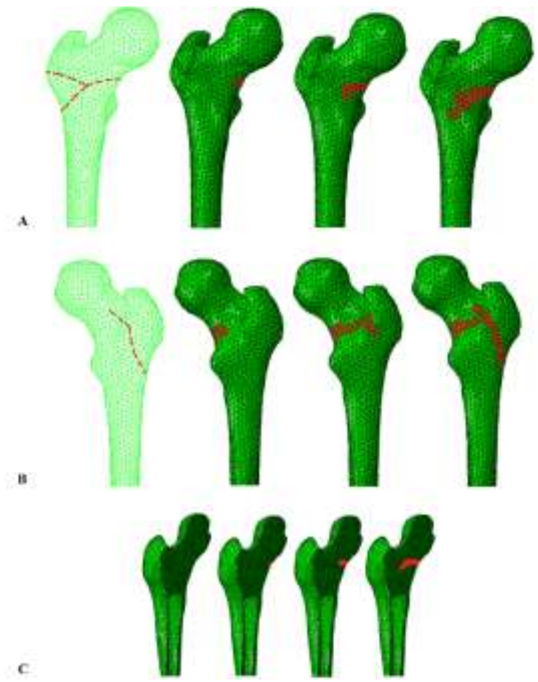

Fig. 6 Experimental crack pattern (left) vs. numerical simulation; anterior (A) and posterior (B) views; C) Numerical simulation of crack propagation in trabecular region

Fig.7 presents the contours of the value of failure function F in compression regime, cf. eq. (3); the latter incorporating the microstructure tensor approach. Again, both the posterior and anterior views are provided of the whole bone. It is evident that the values of this function remain within the range of F<0, which indicates that the fracture of the femur is associated here with the tension regime.

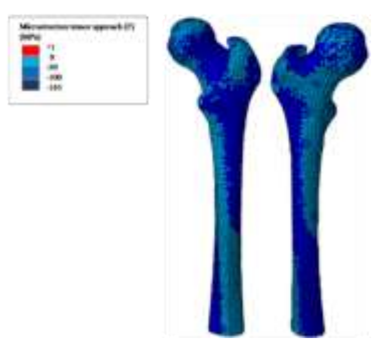

Fig. 7: Contours of failure function in compression regime; posterior and anterior views, respectively

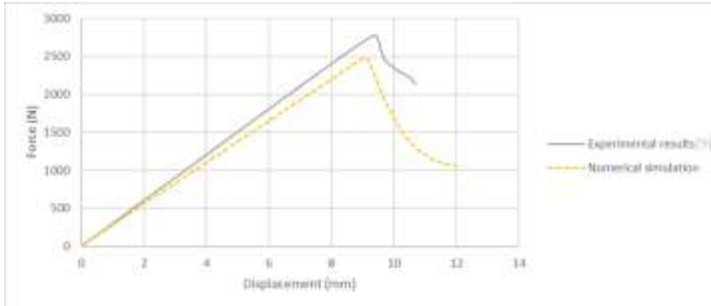

Fig. 8 Load-displacement characteristics for the fracture test; comparison of experimental and numerical results

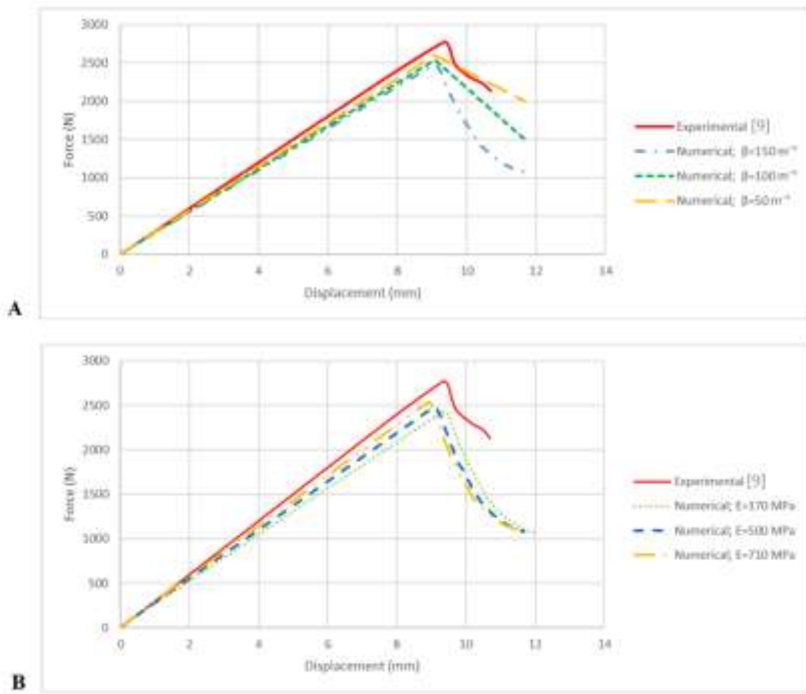

Fig. 9 Parametric studies: A) Load-displacement curves; influence of parameter β , B) Load-displacement curves; influence of Young's modulus E of trabecular bone

The load-displacement characteristics are given in Fig.8. Those correspond to the selected set of parameters, as given in Table 1. The predicted value of ultimate load is close to that recorded experimentally. Given certain ambiguity in selection of elastic constants defining the properties of trabecular bone, as well as the assessment of the rate of softening, a series of parametric studies were conducted. Fig. 9-A shows the sensitivity of the solution to the value of the parameter β , eq.(11). It is evident that this parameter affects primarily the post-peak response, while the ultimate load is not significantly affected. Finally, Fig. 9-B examines the influence of Young's modulus E of the trabecular bone. The range of variation of E is approx. 440 ± 270 (MPa), as indicated by Keaveny et al. [53]. Therefore, a parametric study was done using the average value of E ± the standard deviation of 270 MPa. It is evident that the change in the value of E within the prescribed range does not affect the load-displacement characteristic of the femur and, in particular, the assessment of the fracture load.

DISCUSSION

In cortical bone, the principal material axes are defined *a priori* and the tissue may, in general, be perceived as transversely isotropic. This is in contrast to trabecular bone, which has a complex microstructure and the analysis requires a specific measure of material fabric [54-56]. In addition, the properties depend not only on the anatomical location but also on the size of the specimen, which poses a significant difficulty in terms of formulation of the problem.

In this work, a recently proposed fracture criterion [46] has been employed to assess the onset of crack propagation in cortical tissue. This criterion has been used for the first time in the context of evaluation of fracture load in a femur bone subjected to a sideways fall. The approach has been quite comprehensive as it involved specification of bone geometry based on clinical CT scan, performing a series of material tests to assign the relevant material properties and the numerical simulations of a fracture test, which involved an advanced procedure for tracing the crack propagation.

The critical plane approach corresponding to Rankine cut-off in tension regime, and Tresca criterion formulated within the microstructure tensor approach were used to assess the plastic admissibility of the stress field. Both criteria take into account the anisotropy of strength properties. The latter is often ignored by researchers in view of complexity of the framework and the difficulties associated with specification of material parameters. The most commonly used anisotropic criteria involve those of Hill [57] and/or Tsai and Wu [35]. The former postulates that the strength in compression and tension regime is the same and identification of parameters requires pure shear tests, in addition to direct compression/tension tests, performed in the principal material configuration. Tsai and Wu criterion, on the hand, is an extension of Hill criterion which employs an invariant form of a quadratic function of stress components and takes into account the difference in strength in compression and tension regime. The conditions at failure are defined as pressure dependent, which is not the case for cortical tissue; this criterion also employs a significant number of material parameters. The methodology advocated in this work is simple in numerical implementation and the procedure for identification of material functions requires a limited number of tests, as explained in Section 3.1.

The material tests on cortical bone tissue conducted in this research were limited to axial tension only. This was primarily due to inability to extract a sufficient number of samples from the mid-diaphysis of the bone. However, as noted earlier, the failure mode of the femur involved brittle fracture associated with the tensile regime, so that an accurate assessment of compressive strength was not critical for the evaluation of the ultimate load. In the tensile tests an imperfection, i.e. a small indentation, was generated in the centre of the sample that triggered the onset of localization in this area. It was noted that without this trigger the failure mode involved formation of a macrocrack in the area adjacent to the grippers, which posed a kinematic constraint and made the results of the tests not fully reliable.

The numerical analysis incorporating the volume averaging approach, as described in Section 2.1.3., incorporates a non-local ‘characteristic dimension’, eq.(9), which renders the results to be virtually mesh independent. This again is in contrast to other approaches, such as element deletion [24] or local continuum frameworks [15, 22, 25] for which the results show a pathological mesh-dependency. In addition, the framework employed here can be easily implemented in a standard FE platform. This puts it in an advantage over other approaches, such as those incorporating XFE method, as the latter requires additional degrees of freedom and is computationally less efficient [26, 27].

One of the limitations of the present solution is the smeared nature of the predicted fracture pattern. A more accurate representation would require a discrete tracing of the crack trajectory. This however would drastically increase the computational cost and, at the same time, would not significantly affect the assessment of the ultimate load [58]. It should also be noted that the sideways fall may, in general, involve an impact load that would require a dynamic analysis. For the latter, however, the notion of the rate-sensitivity of the material needs to be properly investigated in order to provide a reliable solution to the boundary-value problem.

The other aspect that needs to be addressed more comprehensively is the influence of the trabecular tissue. As mentioned earlier this is a complex problem that requires an independent study in relation to description of heterogeneity and anisotropy of this tissue. While the mechanical competence of the femur is mainly attributed to the stronger cortical bone, the cancellous tissue may pose some resistance to crack propagation through the trabecular region. Hence, this issue should be investigated in more depth in future studies. Finally, Fig.7 shows the verification of plastic admissibility of the stress state in compression regime. The picture shows the contours of the failure function F based on the microstructure tensor approach, eq. (3), which governs the onset of cracking. The values of this function remain within the range $-185\,\text{MPa} > F > -10\,\text{MPa}$, which indicates that no fracture occurs in compression regime and the only failure mode involved is a brittle tensile fracture. The proposed assessment is numerical simple and, at the same time, has the physical basis.

REFERENCES

[1] O. Johnell and J. A. Kanis, “An estimate of the worldwide prevalence and disability associated with osteoporotic fractures,” *Osteoporos. Int.*, vol. 17, no. 12, pp. 1726–1733, 2006.

[2] L. Cristofolini, M. Juszczyk, S. Martelli, F. Taddei, and M. Viceconti, “In vitro replication of spontaneous fractures of the proximal human femur,” *J. Biomech.*, vol. 40, pp. 2837–2845, 2007.

[3] J. Parkkari *et al.*, “Majority of hip fractures occur as a result of a fall and impact on the greater trochanter of the femur: A prospective controlled hip fracture study with 206 consecutive patients,” *Calcif. Tissue Int.*, vol. 65, pp. 183–187, 1999.

[4] F. Eckstein *et al.*, “Reproducibility and side differences of mechanical tests for determining the structural strength of the proximal femur,” *J. Bone Miner. Res.*, vol. 19, no. 3, pp. 379–385, 2004.

[5] J. H. Keyak, “Relationships between femoral fracture loads for two load configurations,” *J. Biomech.*, vol. 33, pp. 499–502, 2000.

[6] E. M. Lochmüller, O. Groll, V. Kuhn, and F. Eckstein, “Mechanical strength of the proximal femur as predicted from geometric and densitometric bone properties at the lower limb versus the distal radius,” *Bone*, vol. 30, no. 1, pp. 207–216, 2002.

[7] A. C. Laing and S. N. Robinovitch, "The force attenuation provided by hip protectors depends on impact velocity , pelvic size , and soft tissue stiffness," *J. Biomech. Eng.*, vol. 130, pp. 0610051–0610059, 2008.

[8] S. Gilchrist, P. Guy, and P. A. Cripton, "Development of an inertia-driven model of sideways fall for detailed study of femur fracture mechanics," *J. Biomech. Eng.*, vol. 135, pp. 1210011–1210018, 2013.

[9] F. Jazinizadeh, H. Mohammadi, and C. E. Quenneville, "Comparing the fracture limits of the proximal femur under impact and quasi-static conditions in simulation of a sideways fall," *J. Mech. Behav. Biomed. Mater.*, vol. 103, p. 103593, 2020.

[10] M. Bessho, I. Ohnishi, J. Matsuyama, T. Matsumoto, K. Imai, and K. Nakamura, "Prediction of strength and strain of the proximal femur by a CT-based finite element method," *J. Biomech.*, vol. 40, pp. 1745–1753, 2007.

[11] E. Schileo, F. Taddei, L. Cristofolini, and M. Viceconti, "Subject-specific finite element models implementing a maximum principal strain criterion are able to estimate failure risk and fracture location on human femurs tested in vitro," *J. Biomech.*, vol. 41, pp. 356–367, 2008.

[12] D. D. Cody, G. J. Gross, F. J. Hou, H. J. Spencer, S. A. Goldstein, and D. P. Fyhrie, "Femoral strength is better predicted by finite element models than QCT and DXA," *J. Biomech.*, vol. 32, pp. 1013–1020, 1999.

[13] L. Duchemin, D. Mitton, E. Jolivet, V. Bousson, J. D. Laredo, and W. Skalli, "An anatomical subject-specific FE-model for hip fracture load prediction," *Comput. Methods Biomech. Biomed. Engin.*, vol. 11, no. 2, pp. 105–111, 2008.

[14] E. Schileo, F. Taddei, A. Malandrino, L. Cristofolini, and M. Viceconti, "Subject-specific finite element models can accurately predict strain levels in long bones," *J. Biomech.*, vol. 40, pp. 2982–2989, 2007.

[15] E. D. Ara, B. Luisier, R. Schmidt, F. Kainberger, P. Zysset, and D. Pahr, "A nonlinear QCT-based finite element model validation study for the human femur tested in two configurations in vitro," *Bone*, vol. 52, pp. 27–38, 2013.

[16] J. H. Keyak, S. A. Rossi, K. A. Jones, C. M. Les, and H. B. Skinner, "Prediction of fracture location in the proximal femur using finite element models," *Med. Eng. Phys.*, vol. 23, pp. 657–664, 2001.

[17] D. Dragomir-Daescu *et al.*, "Robust QCT/FEA models of proximal femur stiffness and fracture load during a sideways fall on the hip," *Ann. Biomed. Eng.*, vol. 39, no. 2, pp. 742–755, 2011.

[18] L. Grassi *et al.*, "Accuracy of finite element predictions in sideways load configurations for the proximal human femur," *J. Biomech.*, vol. 45, no. 2, pp. 394–399, 2012.

[19] J. E. M. Koivumäki *et al.*, "Ct-based finite element models can be used to estimate experimentally measured failure loads in the proximal femur," *Bone*, vol. 50, pp. 824–829, 2012.

[20] J. C. Lotz, E. J. Cheal, and W. C. Hayes, “Fracture prediction for the proximal femur using finite element models : Part I — linear analysis,” *J. Biomech. Eng.*, vol. 113, pp. 353–360, 1991.

[21] J. C. Lotz, E. J. Cheal, and W. C. Hayes, “Fracture prediction for the proximal femur using finite element models: Part II — nonlinear analysis,” *J. Biomech. Eng.*, vol. 113, pp. 361–365, 1991.

[22] A. Ural, P. Bruno, B. Zhou, X. T. Shi, and X. E. Guo, “A new fracture assessment approach coupling HR-pQCT imaging and fracture mechanics-based finite element modeling,” *J. Biomech.*, vol. 46, no. 7, pp. 1305–1311, 2013.

[23] A. Ural and S. Mischinski, “Multiscale modeling of bone fracture using cohesive finite elements,” *Eng. Fract. Mech.*, vol. 103, pp. 141–152, 2013.

[24] R. Hambli, “A quasi-brittle continuum damage finite element model of the human proximal femur based on element deletion,” *Med. Biol. Eng. Comput.*, vol. 51, pp. 219–231, 2013.

[25] R. Hambli, A. Bettamer, and S. Allaoui, “Finite element prediction of proximal femur fracture pattern based on orthotropic behaviour law coupled to quasi-brittle damage,” *Med. Eng. Phys.*, vol. 34, no. 2, pp. 202–210, 2012.

[26] M. Marco, E. Giner, R. Larraínzar-garijo, J. R. Caeiro, and M. H. Miguélez, “Numerical modelling of femur fracture and experimental validation using bone simulant,” *Ann. Biomed. Eng.*, vol. 45, no. 10, pp. 2395–2408, 2017.

[27] M. Marco, E. Giner, J. R. Caeiro-rey, M. H. Miguélez, and R. Larraínzar-garijo, “Numerical modelling of hip fracture patterns in human femur,” *Comput. Methods Programs Biomed.*, vol. 173, pp. 67–75, 2019.

[28] A. A. Ali *et al.*, “Specimen-specific modeling of hip fracture pattern and repair,” *J. Biomech.*, vol. 47, no. 2, pp. 536–543, 2014.

[29] K. Piekarski, “Analysis of bone as a composite material,” *Int. J. Eng. Sci.*, vol. 11, no. 6, pp. 557–565, 1973.

[30] I. Jäger and P. Fratzl, “Mineralized collagen fibrils: A mechanical model with a staggered arrangement of mineral particles,” *Biophys. J.*, vol. 79, no. 4, pp. 1737–1746, 2000.

[31] H. Gao, B. Ji, I. L. Jager, E. Arzt, and P. Fratzl, “Materials become insensitive to flaws at nanoscale: Lessons from nature,” *Proc. Natl. Acad. Sci. U. S. A.*, vol. 100, no. 10, pp. 5597–5600, 2003.

[32] H. C. Park and R. S. Lakes, “Cosserat micromechanics of human bone: strain redistribution by a ydration sensitive constituent,” *J. Biomech. Eng.*, vol. 19, no. 5, pp. 385–397, 1986.

[33] S. C. Cowin, “Bone poroelasticity,” *J. Biomech.*, vol. 32, pp. 217–238, 1999.

[34] S. Pietruszczak and K. Gdela, “Inelastic analysis of fracture propagation in distal radius,” vol. 77, no. January, pp. 1–10, 2010.

[35] S. W. Tsai and E. M. Wu, “A general theory of strength for anisotropic materials,” *J. Compos. Mater.*, vol. 5, no. 1, pp. 58–80, 1971.

[36] S. C. Cowin, “Fabric dependence of an anisotropic strength criterion,” *Mech. Mater.*, vol. 5, pp. 251–260, 1986.

[37] S. Pietruszczak, D. Inglis, and G. N. Pande, “A fabric-dependent fracture criterion for bone,” *J. Biomech.*, vol. 32, no. 10, pp. 1071–1079, 1999.

[38] C. M. Fenech and T. M. Keaveny, “A Cellular Solid Criterion for Predicting the Axial-Shear Failure Properties of Bovine Trabecular Bone,” *J. Biomech. Eng.*, vol. 121, pp. 414–422, 1999.

[39] W. C. Hayes and T. M. Wright, “An empiricl strength theory for compact bone,” *Fracture*, vol. 3, pp. 1173–1179, 1977.

[40] S. C. Cowin, “On the Strength Anlsotropy of Bone and Wood,” *J. Appl. Mech.*, vol. 46, pp. 832–838, 1979.

[41] L. Rincón-Kohli and P. K. Zysset, “Multi-axial mechanical properties of human trabecular bone,” *Biomech. Model. Mechanobiol.*, vol. 8, no. 3, pp. 195–208, 2009.

[42] K. M. Fox, J. Magaziner, J. R. Hebel, J. E. Kenzora, and T. M. Kashner, “Intertrochanteric versus femoral neck hip fractures: Differential characteristics, treatment, and sequelae,” *J. Gerontol. Med. Sci.*, vol. 54, no. 12, pp. M635–M640, 1999.

[43] Z. Yosibash, N. Trabelsi, and C. Milgrom, “Reliable simulations of the human proximal femur by high-order finite element analysis validated by experimental observations,” *J. Biomech.*, vol. 40, pp. 3688–3699, 2007.

[44] S. Pietruszczak and Z. Mroz, “On failure criteria for anisotropic cohesive-frictional materials,” *Int. J. Numer. Anal. Methods Geomech.*, vol. 25, no. 5, pp. 509–524, 2001.

[45] S. Pietruszczak, “On homogeneous and localized deformation in water-infiltrated soils,” *Int. J. Damage Mech.*, vol. 8, no. 3, pp. 233–253, 1999.

[46] H. Mohammadi and S. Pietruszczak, “Experimental and analytical study of anisotropic strength properties of bovine cortical bone,” *Biomech. Model. Mechanobiol.*, 2020.

[47] S. Pietruszczak, *Fundamentals of Plasticity in Geomechanics*. CRC Press, 2010.

[48] D. T. Reilly and A. H. Burstein, “The elastic and ultimate properties of compact bone tissue,” *J. Biomech.*, vol. 8, no. 6, pp. 393–405, 1975.

[49] E. Novitskaya *et al.*, “Recent advances on the measurement and calculation of the elastic moduli of cortical and trabecular bone : a review,” *Theor. Appl. Mech.*, vol. 38, no. 3, pp. 209–297, 2011.

[50] R. Krone and P. Schuster, “An Investigation on the Importance of Material Anisotropy in Finite-Element Modeling of the Human Femur,” *SAE Int.*, vol. 01, pp. 1–9, 2006.

[51] M. Kutz, *Standard handbook of biomedical engineering and design*. McGraw-Hill, 2002.

[52] H. Mohammadi and S. Pietruszczak, "Description of damage process in fractured rocks," *Int. J. Rock Mech. Min. Sci.*, vol. 113, pp. 295–302, 2019.

[53] T. M. Keaveny, E. F. Morgan, G. L. Niebur, and O. C. Yeh, "Biomechanics of trabacular bone," *Annu. Rev. Biomed. Eng.*, vol. 3, pp. 307–333, 2001.

[54] A. Odgaard, "Three-dimensional methods for quantification of cancellous bone architecture," *Bone*, vol. 20, no. 4, pp. 315–328, 1997.

[55] T. H. Smit, E. Schneider, and A. Odgaard, "Star length distribution : a volume-based concept for the characterization of structural anisotropy," *J. Microsc.*, vol. 191, no. 3, pp. 249–257, 1998.

[56] D. Inglis and S. Pietruszczak, "Characterization of anisotropy in porous media by means of linear intercept measurements," *Int. J. Solids Struct.*, vol. 40, no. 5, pp. 1243–1264, 2003.

[57] R. Hill, *The Mathematical Theory of Plasticity*. Oxford University Press, London., 1950.

[58] E. Haghighat and S. Pietruszczak, "On modeling of fractured media using an enhanced embedded discontinuity approach," vol. 6, pp. 10–22, 2016.

5 Conclusions and future work

In this section a summary of main conclusions, together with some suggestions for future work are provided. It should be noted that a more in-depth discussion pertaining to advantages and limitations of the proposed approaches is given in the papers that form separate chapters of this thesis. It should also be pointed out that, given the format of this article-based thesis, there has been some overlap in terms of description of the methodology; this, unfortunately, is inevitable.

5.1 Concluding remarks

Based on a wide range of numerical simulations presented in this work, the enhanced embedded discontinuity scheme is a very effective tool for describing the mechanical response in the presence of discontinuities within the domain. Unlike other computational methodologies for modelling crack propagation i.e. the strong discontinuity approach and the extended finite element method, the proposed framework requires no special modifications, such as extra degrees of freedom and/or modification of the shape functions. This not only simplifies implementation in the finite elements analysis, but also increases the numerical efficiency, which is of great value in analysis of large scale problems.

As discussed in Chapter 2, the embedded discontinuity approach requires information on the properties of all constituents (i.e. the intact and interface material) and incorporates a non-local 'characteristic dimension'. The latter ensures the objectivity of the solution with regard to discretization. The approach is capable of describing the response in the presence of pre-existing fractures allowing, at the same time, for the onset and propagation of new cracks. The latter has a significant impact on the value of the sample's compressive strength.

As stated in Chapter 3, the shear strength of cortical bone tissue is usually measured by an indirect method using structural tests such as 3-point bending, torsion, and/or tension of specimens with asymmetric double-notch. The interpretation of the results of such experiments is not clear as they constitute *boundary value problems*. Employing the *material testing* is a more reliable and effective way to determine the strength. In a material test the boundary conditions should remain uniform, and the sample's volume should be large compared to its microstructure. In that case, the stress state at the macroscale may be interpreted as homogeneous in a statistical sense.

The experimental work discussed in Chapter 3 included a set of material tests that were carried out using a direct shear apparatus. The key purpose was to examine the sensitivity of shear strength to the normal stress, for different orientations of the sample microstructure. The findings indicate that the shear strength is independent of the normal stress. Thus, the first stress invariant does not influence the conditions at failure *in compression* regime; the strength, however, depends on the orientation of material axis relative to the principal stress system. There are two reasons for the strength pressure-insensitivity. First, the low porosity of the material and second, the existence of the fluid phase, i.e. the generation of excess fluid pressure which restricts the pore space compressibility. The experiments conducted in this work have also shown that the strength of the specimen is significantly reduced in the tension regime, and it is also influenced by the orientation of the sample.

As discussed in Chapter 4, in cortical bone the principal material axes are defined *a priori* and the tissue may generally be interpreted as transversely isotropic. On the other hand, trabecular bone, has a complicated microstructure and its study must involve a specific measure of material fabric. Furthermore, the properties depend not just on the anatomical position but also on the size of the specimen, which presents a substantial challenge in terms of formulation of the problem.

To determine the plastic admissibility of the stress field, the critical plane approach incorporating Rankine cut-off in tension regime and Tresca criterion formulated within the microstructure tensor approach were used. Both criteria take into account the anisotropy of strength properties. The approach advocated in this study is pragmatic and requires a limited number of tests to define the material functions.

As mentioned earlier, the volume averaging method, incorporates a non-local 'characteristic element' that allows the solution to be virtually mesh-independent. This again is in contrast to other methods, such as deletion of elements or local continuum frameworks, for which the results indicate a pathological mesh-dependence. Furthermore, the framework used here can be easily implemented in a standard FE platform. This puts it in advantage over other methods, such as XFEM, as the latter requires additional degrees of freedom and is less efficient in computational terms.

5.2 Suggestions for future work

The current research can be enhanced in several aspects. In relation to Chapter 2, it may be useful to formulate the problem involving the existence of multiple intersecting cracks within XFEM framework and to compare the results with CLED approach. In this case, a new UEL subroutine needs to be developed and implemented in Abaqus in order to use XFE platform for the simulations. For Chapter 3, one of the future directions would be to perform the same series of experimental tests on small samples of the *human* femoral cortical bone. The latter has, in general, a different microstructural arrangement, so that the notions of pressure insensitivity of conditions at failure and anisotropy of strength need to be independently verified.

With regards to Chapter 4, it would be interesting to extend the study to examine the bone-implant interaction. In particular, the performance of various implant designs under different physiological loads could be investigated by employing the methodology outlined in that chapter. Additional research could also be conducted in relation to modeling of mechanical properties of trabecular bone tissue. The last, but not least, the study could be extended to consider discrete crack propagation mode in the 3D model of femoral bone.